# Large-Eddy Simulations of Radiatively Driven Convection: Sensitivities to the Representation of Small Scales

Bjorn Stevens, Chin-Hoh Moeng, and Peter P. Sullivan

*National Center for Atmospheric Research,\* Boulder, Colorado*

## ABSTRACT

Large-eddy simulations of a smoke cloud are examined with respect to their sensitivity to small scales as manifest in either the grid spacing or the subgrid-scale (SGS) model. Calculations based on a Smagorinsky SGS model are found to be more sensitive to the effective resolution of the simulation than are calculations based on the prognostic turbulent kinetic energy (TKE) SGS model. The difference between calculations based on the two SGS models is attributed to the advective transport, diffusive transport, and/or time-rate-of-change terms in the TKE equation. These terms are found to be leading order in the entrainment zone and allow the SGS TKE to behave in a way that tends to compensate for changes that result in larger or smaller resolved scale entrainment fluxes. This compensating behavior of the SGS TKE model is attributed to the fact that changes that reduce the resolved entrainment flux (viz., values of the eddy viscosity in the upper part of the PBL) simultaneously tend to increase the buoyant production of SGS TKE in the radiatively destabilized portion of the smoke cloud. Increased production of SGS TKE in this region then leads to increased amounts of transported, or fossil, SGS TKE in the entrainment zone itself, which in turn leads to compensating increases in the SGS entrainment fluxes. In the Smagorinsky model, the absence of a direct connection between SGS TKE in the entrainment and radiatively destabilized zones prevents this compensating mechanism from being active, and thus leads to calculations whose entrainment rate sensitivities as a whole reflect the sensitivities of the resolved-scale fluxes to values of upper PBL eddy viscosities.

## 1. Introduction

In this paper we report on a series of large-eddy simulations (LES) of an idealized PBL driven by radiative cooling from the top of a radiatively opaque layer of fluid—a smoke cloud. The purpose of our study is to explore and understand the sensitivity of LES to small scales, as manifest in either the resolution of the mesh or the model of subgrid-scale (SGS) motions. The smoke cloud is studied because we find that it retains sensitivities that we have also found to be evident in simulations of stratocumulus (Stevens et al. 1998) and because by only representing the essential features of radiatively driven stratocumulus, without the complications associated with the generation or consumption of latent heat through cloud microphysical processes (e.g., Lilly 1968; Moeng and Schumann 1991; Bretherton et al. 1999), it is somewhat simpler.

The smoke cloud PBL that we consider in this paper is the one proposed by Bretherton et al. (1999). A complicating, albeit realistic and physically interesting, characteristic of this experiment, as opposed to a typical clear convective boundary layer (CBL), is that the degree of stable stratification between the turbulent and quiescent layers is large when compared to the vigor of the underlying turbulence. Typically this aspect of the flow is measured in terms of a bulk Richardson number (e.g., Deardorff et al. 1980; Turner 1986), $Ri_B$:

$$Ri_B = \frac{gz_i\Delta\Theta}{\Theta_0 w_s^2},  \qquad (1)$$

where $z_i$ is the depth of the turbulent layer, $\Delta\Theta$ characterizes the temperature jump between the two layers, $w_s$ is a scale velocity characterizing the turbulent fluid, and $g/\Theta_0$ is the ratio of gravity to a reference temperature.[1] In the smoke cloud experiment $Ri_B > 200$; such

*Corresponding author address:* Mr. Bjorn Stevens, Dept. of Atmospheric Sciences, University of California, Los Angeles, Los Angeles, CA 90095.
E-mail: bstevens@atmos.ucla.edu

[1] $Ri_B$ is similar to the inverse of the square of the bulk Froude Number as earlier defined by Rouse and Dodu (1955). If the generic scale velocity used in Eq. (1) is replaced by Deardorff's convective scale velocity, then our $Ri_B$ is identical to Deardorff's $Ri_*$. For most definitions of a $\Theta_*$ (the convective temperature scale), $Ri_B = \Delta\Theta/\Theta_*$.

large values of $Ri_B$ are typical of stratocumulus but more than an order of magnitude greater than what is commonly found in the CBL. One reason for this is that, in contrast to the CBL, in radiatively driven convection the driving force of the turbulence, that is, cooling of air at cloud top, cooperates with turbulent processes to promote the development of sharp strong inversions. Sharp, strong inversions across which fluxes diverge significantly are often difficult to resolve and thus pose special numerical difficulties. But because sharp, strong inversions are common in stratocumulus boundary layers that have been frequently studied with LES, we are interested in understanding, in some generic sense, the behavior of LES under such conditions.

The smoke cloud has recently come under intense study using both LES and laboratory analogs, and results now emerging in the literature are somewhat in conflict. A key result of the laboratory work is that for such high $Ri_B$ flows, the nondimensional entrainment rate is a function of the Prandtl number of the fluid (Sayler and Breidenthal 1998). The interpretation of this result is that entrainment across the strongly stratified interface, which separates the turbulent fluid from the quiescent fluid, depends on the diffusive thickening (through molecular processes) of the stratified layer, that is, Taylor layers. The conclusion that the thickness of the Taylor layers regulates the entrainment rates in high $Ri_B$ flows is troubling for LES, which by nature assumes that molecular processes are inconsequential. Just how troubling this is remains uncertain, mostly because the laboratory results can be questioned on many grounds: they are low Reynolds number, the low aspect ratio of the container may bias the problem, container scale circulations may affect physical processes, and differences in how the radiative forcing is applied may affect the analogy between the laboratory flow and the LES. Thus, despite the fact that the laboratory experiments represent a real flow, it is not obvious that such experiments are any better at representing the hypothetical smoke cloud than is LES.

LESs of the smoke cloud are not only in conflict with the low Reynolds number laboratory data, they also disagree among themselves. While there is general agreement that fine vertical resolution is needed to properly represent processes at the entrainment interface (e.g., Bretherton et al. 1999; Stevens and Bretherton 1999; Lewellen and Lewellen 1998; Lock and MacVean 1999; vanZanten et al. 1999; also see section 2 and appendix C of this article), there is disagreement as to the importance of small-scale turbulence as manifest in sensitivities to horizontal resolution or SGS model assumptions.[2] For instance, simulations by the Lawrence

---

[2] In discussions of LES results we often use the words small scales to refer to scales on the order of the grid scale, which is orders of magnitude larger than the viscous or diffusive scales postulated to be important in low Reynolds number high $Ri_B$ laboratory flows.
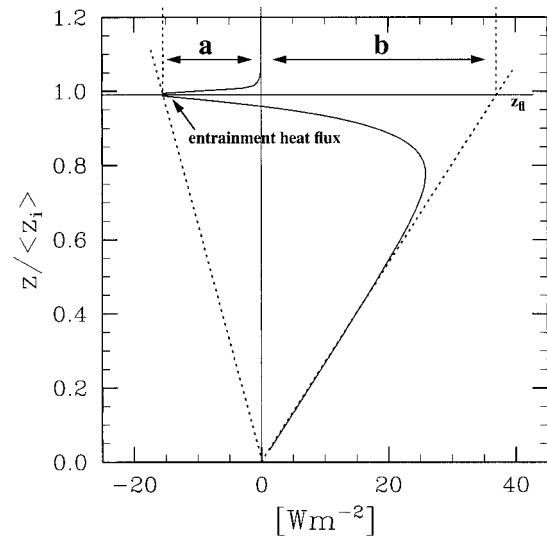


FIG. 1. Heat flux from LES showing the relationship between the entrainment heat flux and the extrapolated heat flux used in process partitioning parameterizations of entrainment.

Berkeley Labs–University of Washington (LBL–UW) group (Stevens and Bretherton 1999) display an explicit sensitivity to the horizontal resolution for weakly stratified experiments (small $Ri_B$); in contrast, simulations by the West Virginia University (WVU) group (Lewellen and Lewellen 1998) are remarkable in their lack of sensitivity to horizontal resolution even for strongly stratified interfaces (large $Ri_B$). Thus while the range of resolved scales appears to be important in determining the entrainment rate in the LBL–UW LES, this is not the case for the LES by the WVU group.

Further disagreement among LES is also evident in recently published entrainment relationships (Lewellen and Lewellen 1998; Lock and MacVean 1999; vanZanten et al. 1999). Both the Lewellen and Lewellen and the vanZanten et al. studies have proposed that process partitioning provides a rational framework for describing entrainment rates deduced from LES. Roughly speaking, for the smoke cloud this closure assumption can be interpreted as stating that the extrapolated buoyancy flux in an entraining PBL (denoted by ''b'' in Fig. 1) is a fixed fraction of what it would be in the absence of entrainment. In other words, process partitioning closures predict that $b/(a + b)$ or simply $a/b$ is a universal constant. Although calculations by a number of groups suggest that their respective simulations are well constrained by such a relationship, the entrainment relations are, to a certain extent, model dependent. For instance, the IMAU (vanZanten et al. 1999) and the WVU (Lewellen and Lewellen 1998) groups predict $a/b \approx 0.4$, while the UKMO group (Lock and MacVean 1999) predicts $a/b$ closer to 0.2. Scatter in the relationships among the models tends to be larger than the scatter associated with any one model, which suggests that the precision

of an individual simulation is much greater than its accuracy.

Thus recent studies raise many questions: Do the entrainment relationships found by various groups to describe the behavior of large $Ri_B$ flows reflect real physical relationships? If so, what is the physical character of these relationships, and what physical processes do they underscore? Moreover, if the LES results reflect real physical processes, what explains the scatter among the various calculations? Why are calculations by some groups extraordinarily robust as a function of horizontal resolution while others are not? And how can the LES be reconciled with previous laboratory and experimental work? In this paper we begin to take a crack at some of these important and outstanding questions. We do so by attempting to summarize what ended up being scores of simulations, with two independently developed codes, on $64 \times 64 \times 71$ grids or larger. Our focus will be on the nature of horizontal resolution sensitivities in fine vertical resolution simulations of the smoke cloud and the relationship of such sensitives to SGS models.

## 2. Background

### a. Entrainment rates and fluxes

The focus of this study is on entrainment. For simulations of the cloudy boundary layer this is the single most important parameter of the flow. In a sense it represents an internally determined boundary condition on the turbulent flow. To illustrate this we consider the jump conditions for conserved quantities, as well as quantities with well-behaved forcings. In the limit of vanishing entrainment zone thickness [a limit well approximated in the large $Ri_B$ flow under consideration here, e.g., vanZanten et al. (1999)], any conserved scalar $\phi$ (i.e., one such as the smoke tracer, that satisfies the equation $d\phi/dt = 0$) has fluxes that satisfy the so-called jump condition

$$w_e \Delta \phi = -\overline{w\phi}|_{z=z_i}, \qquad (2)$$

where omitting the large-scale vertical motion, $w_e = dz_i/dt$ is the entrainment rate and $\Delta\phi = \lim_{\epsilon \to 0}[\phi(z_i + \epsilon) - \phi(z_i - \epsilon)]$ is the jump of $\phi$ across the inversion. Equation (2) is a simple rephrasing of the conservation equation for $\phi$ in a vanishingly thin control volume whose base is at $z_i$ (e.g., Kraus 1963; Lilly 1968). Because in a quasi-steady state the fluxes of conserved variables are linear (by definition) the value of the flux everywhere is proportional to the entrainment flux, or the entrainment rate. Consequently, (2) and quasi-steadiness lead to the fact that the flux of the smoke tracer anywhere makes a good proxy for the entrainment rate $w_e$.

A relationship such as the one given in Eq. (2) can also be formulated for nonconservative variables, so long as the source terms for these variables are integrable across the control volume (e.g., Moeng et al.

TABLE 1. Initial sounding. In all cases the mean wind and all surface fluxes are set to zero.

| Height | $\theta$ | $s$ |
|---|---|---|
| 0.0 | 288.000 | 1.0 |
| 687.5 | 288.000 | 1.0 |
| 712.5 | 295.000 | 0. |
| 2212.5 | 295.156 | 0. |

1999). For the case of the smoke cloud, the only diabatic process is radiation, in which case the jump condition for potential temperature, $\theta$, takes the form:

$$w_e \Delta\theta = -\overline{w\theta}|_{z=z_i} + \frac{1}{\rho_0 c_p}\Delta F, \qquad (3)$$

where $\Delta F$ describes the change in the radiative flux across the inversion. As long as $\Delta F$ is fixed and the entrainment zone remains thin, this relationship shows that there is a direct relationship between $\overline{w\theta}|_{z=z_i}$ and entrainment. By design (see section 2), these conditions are usually met in our simulations, consequently we often speak of, or examine, the entrainment heat flux as a surrogate for the entrainment rate itself in flows with a given $\Delta\Theta$. In summary, the above relationships illustrate how in the limit of thin entrainment interfaces $w_e$ determines, in part or in whole, all fluxes at the top of the PBL, and hence is a fundamental parameter of the PBL.

### b. Methods

#### 1) SETUP

A description of the experimental configuration of LES of the smoke cloud is detailed in Bretherton et al. (1999). For completeness the basic thermodynamic configuration is compiled in Table 1. Unless otherwise stated it is adhered to identically here. Broadly speaking our simulations fall into three classes: SMK-S-064 simulations are smoke cloud calculations based on the Smagorinsky SGS model and with 64 points in each horizontal direction. SMK-T-064 are identically configured calculations except they are based on the Deardorff prognostic turbulent kinetic energy (TKE) SGS model. SMK-S-128 calculations are identical to SMK-S-064 calculations except twice the number of points are used to span the same domain in each horizontal direction. In the future, references to higher-resolution or finer-mesh simulations refer to simulations falling into the SMK-S-128 class. Standard simulations are denoted by the SMK-S-064 class.

All of the results actually presented in this paper are from the Colorado State University (CSU) code (e.g., appendix A) although in some select instances we test the robustness of our ideas using the substantially different nested-mesh, pseudospectral, code developed at the National Center for Atmospheric Research (NCAR; Moeng 1984; Sullivan et al. 1996). For reasons dis-

cussed below, all of the calculations with the CSU model were carried out with a fine (5 m) vertical mesh spanning at least a 100-m zone about the mean inversion.[3] Away from the entrainment zone the mesh is gradually stretched to a maximum $\Delta z = \frac{1}{2}\Delta x$ near the surface and 100 m in the quiescent stratified layer. Tests with a uniformly fine mesh indicate that the method of stretching does not noticeably influence our results.

### 2) Vertical grid spacing

In addressing the sensitivity of LES to the representation of small scales it would seem natural to explore the sensitivity of the simulations to vertical resolution (e.g., Bretherton et al. 1999; Stevens and Bretherton 1999; Lock and MacVean 1999). Indeed, we initially proceeded along these lines, only to find that the resulting sensitivities in our calculations are complicated by the fact that the sharp radiative cooling profile tends to nonlinearly cool the air in the inversion as smoke is diffused into it—leading to larger entrainment rates for increasing resolution. Indeed we have constructed a simple analytical model (included for reference in appendix C) that we believe provides a plausible explanation (solely in terms of radiative effects) for the previously noted sensitivity of entrainment to vertical resolution. Because we believe that previously reported vertical sensitivities are predominantly radiative–dynamical sensitivities, rather than intrinsically dynamical sensitivities, as has been sometimes suggested (e.g., Stevens and Bretherton 1999), and because our interest is in the latter type of interaction (and in particular how it relates to SGS processes), in this paper we do not further pursue questions related to the sensitivity of our simulations to changes in vertical resolution.

Instead we fix the vertical grid spacing about the entrainment zone to be 5 m in all of our calculations. This scale was chosen because (as evident by comparing simulations with 5- and 3-m vertical grids, and as predicted by the analytic model in appendix C) the sensitivity of the calculation to further refinements in the vertical grid tended to be less than the sensitivities that interest us here. Because we used the same vertical grid in all the calculations, and because we did not alter the nature of the radiative flux parameterization [e.g., Eq. (A5)], the amount of radiative cooling in the inversion was approximately fixed in all our calculations; that is, in contrast to other studies where this was not the case, tests show that this effect does not contribute significantly to the sensitivities we explore.

---

### 3) Analysis

Statistics are compared after the simulations achieve a quasi steady state (as measured by the time evolution of the boundary layer turbulent kinetic energy TKE and the linearity of fluxes of conserved quantities). Most statistical quantities (i.e., velocity variances, the mean state, fluxes, and terms in the resolved-scale TKE budget) are computed during the integration at 30-s intervals (approximately every 30 time steps). Inevitably, unanticipated postprocessing is warranted in which case the averages are over a coarser grained time record (every 3 min for 1 h). The results are not particularly sensitive to this degree of refinement in the granularity of the time record.

To make efficient use of limited resources, many simulations are conducted by branching off a control simulation for 90 min of simulated time. Only the last 60 min of a branched integration are analyzed. By studying how flows tended to decorrelate from their initial conditions (or from each other) over this period, we found that our analysis period may begin too soon. This motivated us to selectively test our ideas using integrations started from fresh initial conditions. In these cases the variability among independent realizations, when averaged over the analysis period, was found to be much smaller than the sensitivities we are interested in. As a result we are satisfied that our analysis procedure reveals robust sensitivities of a particular code. The fact that critical conclusions were yet further tested using integrations with a completely different model suggests that our results may even have some degree of generality.

We typically plot fields versus the nondimensional height $z/\langle z_i \rangle$, where angle brackets denote averaging over horizontal planes and time records. For the smoke cloud simulations, $z_i(x, y, t)$ is determined to be the uppermost level at which the smoke concentration falls to one-half its value at the lowest model level; although, as noted in the text, other methods are used at times. Typically our analysis is done by averaging all time records on the computational grid and then interpolating to a $\langle z_i \rangle$ normalized grid. Because $w_e \Delta t \approx 2\Delta z$ (where $w_e$ is the entrainment rate, $\Delta t$ is the analysis period, and $\Delta z = 5$ m is the typical grid spacing at the inversion) our results are not overly sensitive to the method of averaging.

### c. *What does entrainment look like in LES of the smoke cloud?*

Before proceeding with a detailed study, based largely on statistical measures of the flow, it is worthwhile to familiarize ourselves with the structure of the entrainment zone as represented by LES. Figure 2 illustrates the structure of the inversion for a SMK-S-128 simulation with $c_s$ (the length scale coefficient in the Smagorinsky model) equal to 0.23. Many things are apparent in this figure: (i) the thickness of the inversion (as mea-
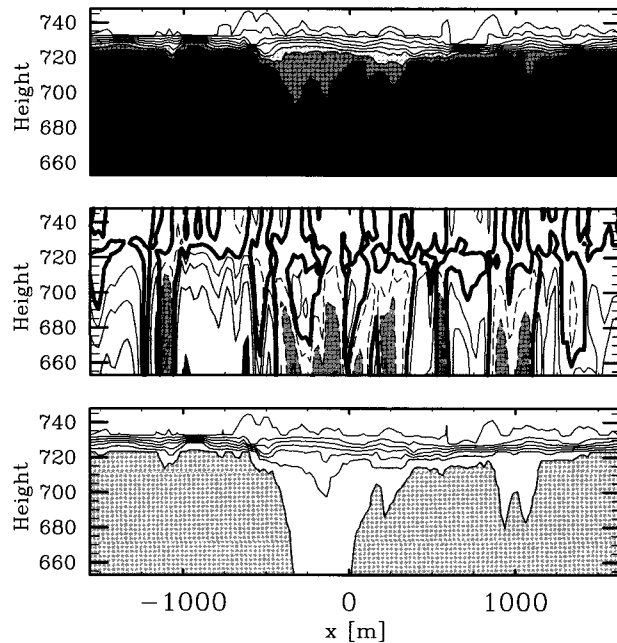
FIG. 2. Snapshots from an SMK-S-128 simulation at $t=9000$ s of $\theta$ (upper panel, contours at 287.5, 288.0, 289.0, 290.0, 291.0, 292.0, 293.0, 294.0, 294.5 K), $w$ (middle panel, contours at $-1.00$, $-0.50$, $-0.25$, $-0.10$, 0.00, 0.10, 0.25, 0.50, 1.00, with negative contours dashed and zero contour thickened), and $s$ (lower panel, contours at 0.05, 0.20, 0.35, 0.50, 0.65, 0.80, 0.95, 0.98, 1.00). Shading is applied to help accentuate features.
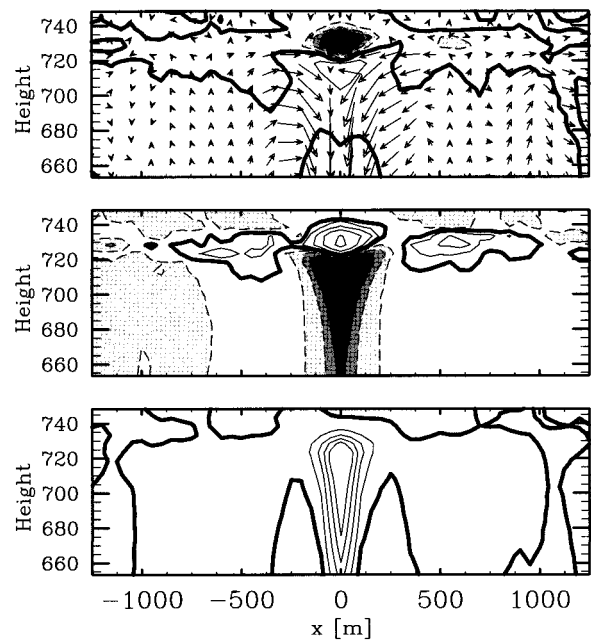
FIG. 3. Conditionally sampled fields from an SMK-S-064 class simulation. The sampling is about downdrafts at $z_c = 0.85z_i$. In defining events we use $d = 0.15z_i$ and a threshold of $1.25\sigma_w$ ($z = z_c$) (see Schmidt and Schumann for more details about the method). Here $\theta$ perturbations (upper panel, contours at $-0.25$, $-0.15$, $-0.10$, $-0.05$, 0.00, 0.05, 0.10, 0.15, 0.25 K), with superposed velocity vectors; smoke concentration perturbations (middle panel, unevenly spaced contours at $-0.0100$, $-0.0050$, $-0.0025$, 0.0000, 0.0025, 0.0050, 0.0100, 0.0200, 0.0400), and $p'$ (lower panel, contours every 0.01). Negative contours are dashed and zero contour is thickened. Shading is applied to help accentuate features.

sured by the distance between smoke or $\theta$ contours) is variable, tending to be thicker above downdrafts; (ii) there is no evidence of contours overturning at the inversion, instead contours tend to be steepened at the edge of updrafts and peeled away at the base of downdrafts; (iii) the inversion height fluctuates only slightly across the domain and the entire jump in $\theta$ often spans no more than one or two grid points; (iv) smoke and $\theta$ contours are well correlated, but because $\theta$ has a source in radiation we do not expect them to be perfectly correlated; (v) thin layers of radiatively cooled air are most evident in the divergent layers above updrafts, and deep layers of radiatively cooled air tend to correlate with downdrafts (e.g., compare Figs. 2a and 2b).

Additional insight is gained through a perusal of conditionally sampled fields, for example, Fig. 3 derived from SMK-S-064 class simulations. The conditional sampling method we use is described by Schmidt and Schumann (1989). Because we are interested in interfacial structure, and its relation to entrainment, we define events based on downdraft velocity at $z_c = 0.85z_i$, using an exclusion distance $d = 0.15z_i$, and a sampling threshold of $w \leq -1.25\sigma_w(z_c)$. The analysis is quantitatively sensitive to choices of thresholds; nonetheless, in conjunction with the snapshots it proves useful in helping one to form at least a qualitative view of entrainment in LES. The analysis shows that the most radiatively destabilized region of the downdraft is off-

axis at the top (or root) of the downdraft. We attribute this to the fact that the downdraft is accelerated by the negative buoyancy of the radiatively cooled air that is converging at its base. In association with this convergence, a high-pressure maximum can be found in the inversion at the root of the downdraft. These high pressure regions are associated with a weak recirculation region that helps thicken the interface (causing the dipole-like structure in the $\theta'$ field at $z_i$), thereby facilitating the incorporation of inversion zone air into the PBL at the downdrafts root.

Figure 4 attempts to encapsulate our provisional view of entrainment in these relatively coarse resolution LES of radiatively driven large $Ri_B$ flows. The main elements of the figure are threefold: the interface is shown to be thinned and thickened by the energy containing large eddies; the pressure maximum lies in the inversion, above the downdraft that incorporates entrained air; the radiatively cooled air initially forms above updrafts and feeds the downdrafts. Associated with the thickened interface and the high pressure region are decelerating interfacial disturbances. On our figure these disturbances are represented as a flapping and steepening of a contour. This simplified representation of interfacial disturbances can be misleading, as often contours within
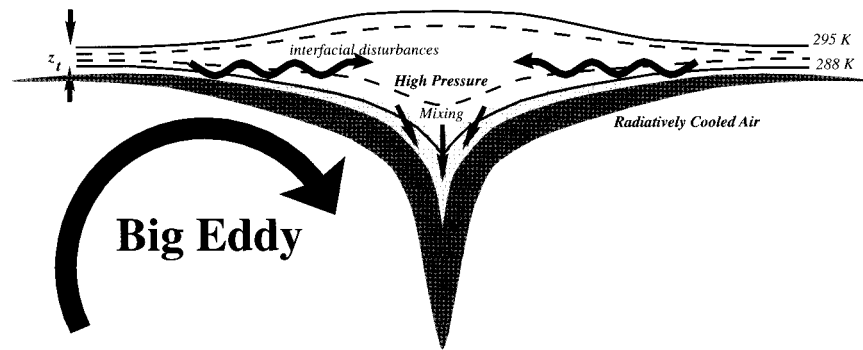
FIG. 4. Schematic figure of the nature of entrainment in a radiatively forced layer as represented by our LES. In part this figure represents the dynamics as we see them superimposed on a conditionally averaged view of the interface.

the inversion are observed to diverge in association with small-scale propagating disturbances.

Unfortunately, it is not straightforward to diagnose the source of entrained air. Because there are small amounts of the radiatively active tracer throughout the inversion, radiative cooling in this layer may still play a small role in setting the entrainment rate, for example, appendix C. In terms of turbulent processes, the simulations show evidence (as noted above) of filaments of inversion air being pulled away from the inversion by the pressure gradient set up by the large eddies. Although this thickening and peeling is also evident in better resolved, lower $Ri_B$ flows (e.g., Sullivan et al. 1998), in our simulations, where $Ri_B$ is large, this process appears more dominant. The agitation of the stable interface by the large eddies results in small-scale interfacial disturbances that propagate in and along the stratified layer. These disturbances converge on and establish the pressure maximum at the root of the downdraft, and perhaps contribute to the thickening and peeling process. While there does appear to be evidence of mixing associated with these propagating disturbances, the lack of resolution frustrates attempts to quantify their role in preconditioning inversion air for subsequent incorporation into the downdraft. Ultimately, to say that entrainment is well resolved, one would like to see a separation of scales between fluid comingling and entrainment—this is not apparent in any of our large $Ri_B$ simulations.

## 3. The effect of horizontal resolution

Similar to the LBL–UW results, but in contrast to those by the WVU group, entrainment rates in calculations with the CSU code are sensitive to horizontal resolution. Figure 5 shows the effect of a doubling of horizontal resolution on the buoyancy and smoke fluxes. We note (in part because it is not obvious from the figure) that the better resolved flow has larger entrainment fluxes. Even less evident from the figure is that when the resolution is doubled changes in the total heat

flux at $z_i$ largely reflect changes in the resolved heat flux at $z_i$.

Changing the horizontal resolution also changes $\lambda$, the mixing length scale used by our parameterization of SGS turbulence (e.g., appendix B). Based on simulations of the small-$Ri_B$ CBL, Mason (1989) argues that specifying values of $c_s$ that differ from the theoretically derived value ($C_s$) essentially sets a filter scale $\lambda_f = c_s \lambda / C_s$, and that simulations with equivalent values of $\lambda_f$ should behave equivalently.[4] Indeed, we see that doubling the resolution (i.e., halving the mesh spacing) and doubling the value of $c_s$ results in fluxes that tend toward the coarse mesh integration. A wider ranging sequence of calculations is described in Table 2. These results suggest that Mason's argument captures the tendency of the simulations, especially in the limit as $\lambda$ goes to zero for a fixed domain size. Indeed, recently Mason and Brown (1999) looked at this issue further for the case of a weakly capped CBL and demonstrated that simulations with $\lambda_f$ fixed tend to converge with increasing $c_s$ reflecting the fact that the actual filter implied by the simulation is determined both by the SGS model and one's choice of numerical methods. Our results tend to support their finding for the case of the smoke cloud. The approximate agreement in entrainment rates for small $\lambda$ (i.e., experiments 304.2 and 302.1) also is reflected by good agreement in the velocity variances (Fig. 6); although there is some indication that higher-order moments retain a sensitivity to $\lambda$ for fixed $\lambda_f$, particularly near the boundaries of the turbulent flow, this might merely reflect the fact that the higher-order moments are more sensitive to finite-differencing errors in these regions. In the end, because the effects of changes to $\lambda$ with fixed $c_s$ are reasonably well captured by simulations in which $\lambda$ is fixed, but $c_s$ is varied, we consider the

---

[4] Here we distinguish between $C_s$ the theoretical value of the Smagorinsky constant, and $c_s$ the value we use in our SGS parameterization.

## (a) $(w\theta)_{\text{tot,sgs}}$ $[\Delta_x\text{-Runs}]$

## (b) $(ws)_{\text{tot,sgs}}$ $[\Delta_x\text{-Runs}]$

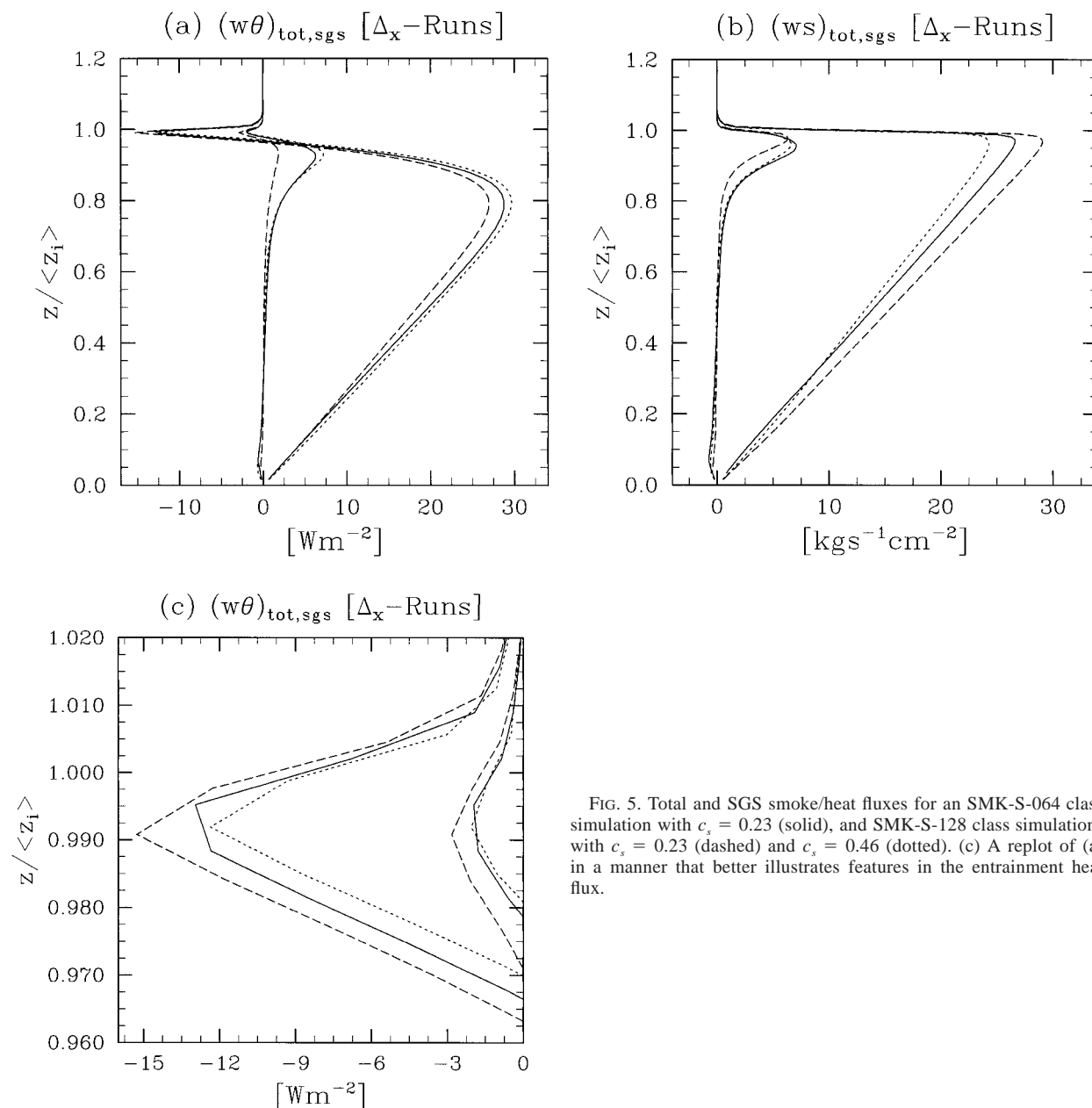## (c) $(w\theta)_{\text{tot,sgs}}$ $[\Delta_x\text{-Runs}]$

Fig. 5. Total and SGS smoke/heat fluxes for an SMK-S-064 class simulation with $c_s = 0.23$ (solid), and SMK-S-128 class simulations with $c_s = 0.23$ (dashed) and $c_s = 0.46$ (dotted). (c) A replot of (a) in a manner that better illustrates features in the entrainment heat flux.

sensitivity to small scales further by studying how changes in the SGS model affect our calculations.

## 4. The Smagorinsky (Lilly) Model

As shown in appendix B, the Smagorinsky model can be viewed as the equilibrium limit of the prognostic SGS–TKE model. Without a length-scale correction for stability it predicts an eddy viscosity and diffusivity of the form

$$K_m = (c_s\lambda)^2 S \sqrt{1 - \frac{\text{Ri}_{\text{D}}}{\text{Ri}_{\text{c}}}}, \qquad K_h = \frac{K_m}{\text{Pr}}, \qquad (4)$$

where

$$S = \left[\frac{\partial \overline{u}_i}{\partial x_j}\left(\frac{\partial \overline{u}_i}{\partial x_j} + \frac{\partial \overline{u}_j}{\partial x_i}\right)\right]^{1/2} \qquad (5)$$

is the magnitude of the deformation; $\lambda$ is a length scale, which we set here to the horizontal grid spacing; $c_s$ is a constant parameter; $\text{Ri}_{\text{D}} = N^2/S^2 = (g/\theta_0)(\partial\overline{\theta}/\partial z)S^{-2}$

TABLE 2. Value of $w_e$ for simulations with differing values of $\lambda$ but with $\lambda_f$ held constant at 50 m.

| Name | $\lambda$ [m] | $w_e$ [mm s$^{-1}$] |
|------|------|------|
| 304.2 | 25 | 2.5 |
| 302.1 | 50 | 2.6 |
| 313.1 | 100 | 3.1 |
| 314.1 | 200 | 3.8 |

is a local SGS (or deformation) Richardson number, and $\mathrm{Ri_c}$ is a critical Richardson number.

For many of the experiments we shall consider $\mathrm{Ri_c}$ and $c_s$ to be free parameters; although, given a number of assumptions as reviewed in the appendix one should set $\mathrm{Ri_c}$ equal to the turbulent Prandtl number, $\mathrm{Pr} \approx 0.3$ and $c_s = C_s = \pi^{-1}[2/(3\alpha)]^{3/4}$, where $\alpha \approx 1.5$ is the Kolmogorov constant. Also recall that because $\mathrm{Ri_c}$ is, from (26), a turbulent Prandtl number, it plays two roles: in unstable conditions it acts like a Prandtl number in that it determines the ratio of buoyancy and shear production of small-scale turbulence, in stable conditions it determines when the buoyancy field will be sufficiently strong to suppress the generation of small-scale turbulence by shear.

In the above form [i.e., Eq. (4)], the Smagorinsky model can be thought of as having two components: a neutral component proportional (by the constant $c_s$) to the magnitude of the deformation and a prefactor, which depends on the local $\mathrm{Ri_D}$. Below our discussion is loosely organized around the respective role of these two terms; although, because the deformation appears in the definition of $\mathrm{Ri_D}$ this separation is only roughly true.

### a. The effect of $c_s$

#### 1) ON ENTRAINMENT RATES AND SCALAR FLUXES

As discussed in the previous section, SMK-S-128 class simulations are sensitive to the value of $c_s$ in the Smagorinsky model (cf. Fig. 5). A similar result is illustrated in Fig. 7, which summarizes SMK-S-064 simulations spanning a broader range in $c_s$.[5] The tendency of calculations with larger values of $c_s$ to have smaller entrainment rates occurs despite the presence of a negative feedback. Less entrainment implies more production of TKE, which should support further entrainment. Presumably, such a feedback would impose a certain amount of rigidity on the flow, thereby lessening the sensitivity of the results to changes in parameters.

The effect of $c_s$ on entrainment rates is largely mediated by changes in the resolved scales. Consider the entrainment heat flux, which we associate with the minimum heat flux located near the inversion. As was discussed in section 2, so long as the radiative flux does not change its shape among the simulations (which to a sufficient degree of approximation is the case in our simulations) the entrainment heat flux is a good proxy for the entrainment rate. That, in an absolute sense, the

---

[5] Strictly speaking values $c_s < C_s$ imply a filter scale smaller than ones grid scale. However, only for such small values of $c_s$ do we generate a $-5/3$ energy spectrum down to the grid scale—a traditional goal in SGS modeling, although as pointed out by Mason and Brown (1999) not necessarily a well-founded one. Larger values of $c_s$ tend to produce spectra that fall off more rapidly. For this reason, and because associating $\lambda$ with $\Delta x$ is only a rough statement of the filter scale, we believe the $c_s = 0.15$ experiments are worth considering.
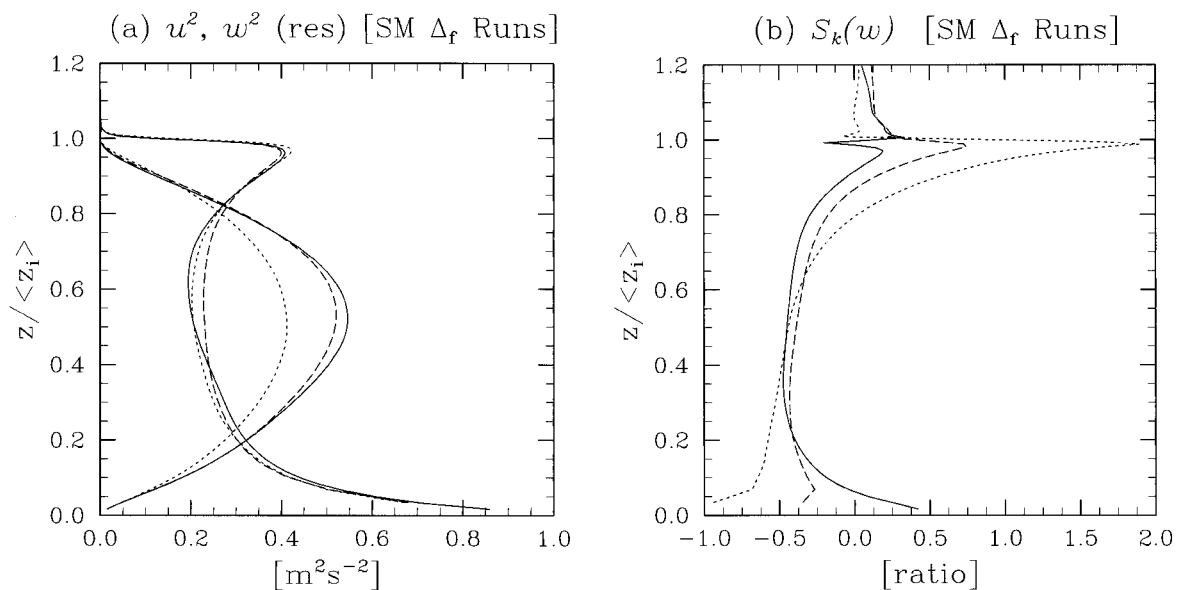


FIG. 6. Sensitivity to $\Delta x$ for fixed $\lambda_f$ for smoke cloud simulations: (a) velocity variances ($w^2$ curves peak near $0.5z/z_i$) and (b) skewness of $w$. Solid line, $\Delta x = 25$ m; dashed line $\Delta x = 50$ m; dotted line $\Delta x = 100$ m.
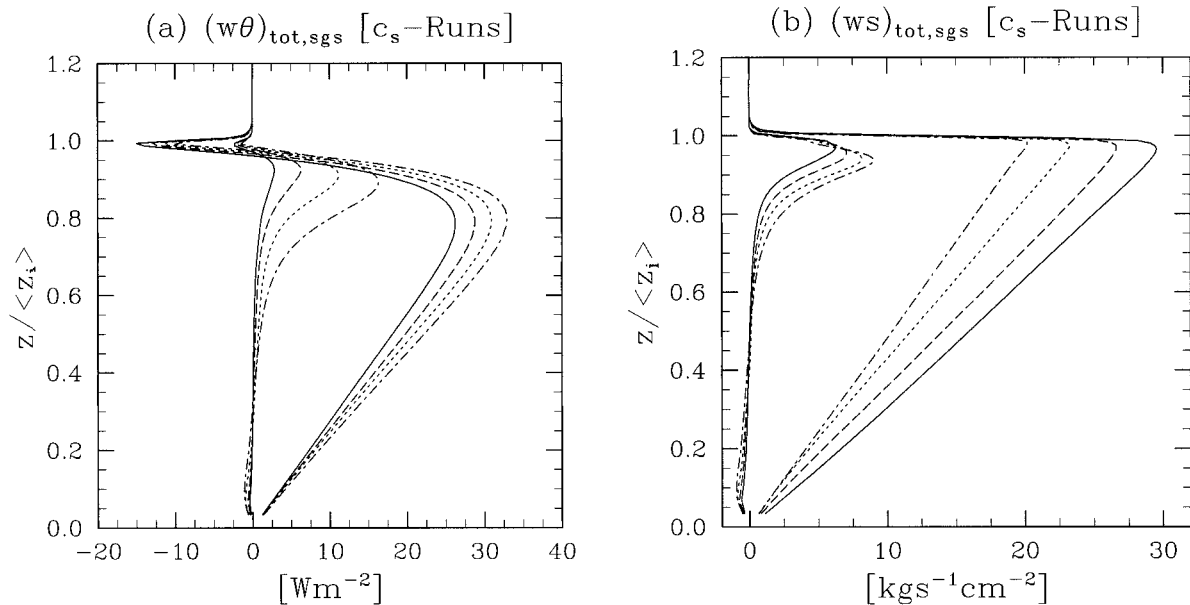
FIG. 7. Smoke cloud sensitivity of (a) theta and (b) smoke fluxes to changes in $c_s$ for a suite of SMK-S-064 class simulations with $c_s = 0.15$ (solid), 0.23 (dashed), 0.35 (dotted), 0.53 (dash–dot).

change in the total entrainment heat flux is mostly accommodated by changes in the resolved scales (or a lack of change in the subgrid scales) is more clearly evident in Table 3, which lists the resolved and SGS contributions to the entrainment heat flux for calculations with varying values of $c_s$ and $\Delta x$.

The reduction of resolved entrainment associated with an increase in $c_s$ is associated with reductions in the near-interfacial values of resolved vertical velocity variance. Figure 8 illustrates how the $c_s = 0.35$ solution has narrower tails in the velocity distribution near the inversion, and also a less agitated inversion (as evidenced by a reduced probability of the inversion being characterized by relatively weak stratification). Conditionally sampled fields and snapshots support this view, wherein larger values of $c_s$ leads to a smoother, more highly organized, flow (i.e., one in which correlations in conditionally sampled fields are stronger).

The cospectra of $w$ and $\theta$ is given by the real part of $\hat{w}\hat{\theta}^*$, where star denotes the complex conjugate and "hat" denotes the Fourier transform. For suitably defined forward transforms the sum over all wavenumbers

TABLE 3. Resolved and SGS heat flux minima (in W m$^{-2}$) for simulations with differing values of $c_s$.

| $c_s$ | $\Delta x$ | $\langle \overline{w\theta} \rangle$ | $\langle w'\theta' \rangle$ |
|---|---|---|---|
| 0.15 | 50 | −12.92 | −2.72 |
| 0.23 | 50 | −11.84 | −2.36 |
| 0.35 | 50 | −10.65 | −2.43 |
| 0.53 | 50 | −9.58 | −1.62 |
| 0.23 | 25 | −13.66 | −2.95 |
| 0.36 | 25 | −12.67 | −2.90 |
| 0.46 | 25 | −11.47 | −2.19 |

of the cospectra is equal to the flux $\overline{w\theta}$. Cospectra of the heat flux at the inversion thus provide insight into how changing $c_s$ modifies the resolved entrainment flux. Plots of the cospectra at the height of the minimum buoyancy flux, and at two levels (10 m) below this height are given in Fig. 9. The fact that $c_s$ preferentially affects the high-wavenumber end of the cospectra is in accord with interpretations of the SGS model as setting an effective filter scale; however, the degree to which modest changes in $c_s$ influence the larger scales is somewhat surprising. The tendency, with increasing $c_s$, of even larger scales to carry most of the flux supports the basic result that entrainment fluxes are increasingly associated with the larger, more organized, scales as $c_s$ is increased.

The view (e.g., Fig. 8) that it is the effect of $c_s$ on the velocity field that is critical in reducing the entrainment rate, and the resolved entrainment heat flux, is further supported by simulations in which $c_s$ is alternately modified in either the eddy viscosity calculation, the eddy-heat diffusivity calculation, or the eddy-smoke diffusivity calculation: changes to the viscosity lead to by far the largest impact on entrainment rates, changes to eddy-heat diffusivities affect entrainment rates only slightly, and changes to the eddy-smoke diffusivity affects entrainment not at all. Still more tests suggest that if $c_s$ is allowed to vary with height, it is the value of $c_s$ in the uppermost part of the PBL that most strongly affects the flow.

### 2) ON SGS FLUX MAXIMA

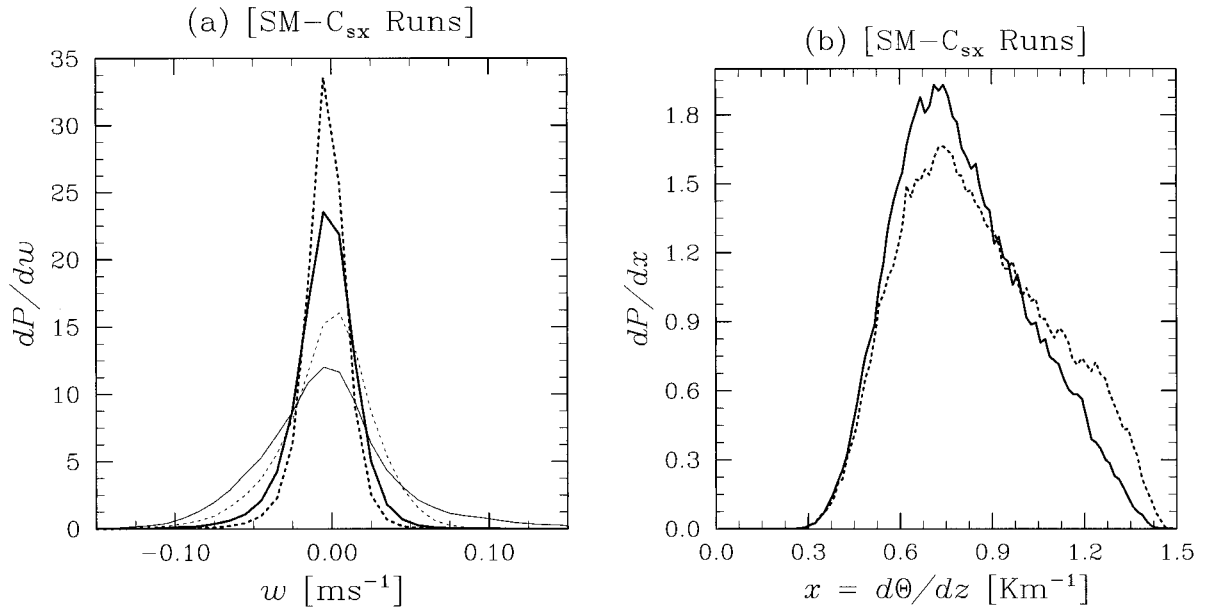As pointed out above, in the current implementation of the model, changing $c_s$ does not significantly affect

FIG. 8. PDFs of (a) $w$ at $z_i$ (thick) and $z_i - \Delta z$ (thin lines) and (b) $(\Delta\theta/\Delta z)_{max}$ for SMK-S-064 class calculations with $c_s = 0.15$ (solid line) and $c_s = 0.35$ (dotted line).

the SGS entrainment heat flux; however, the values of SGS heat fluxes outside of a small neighborhood about $z_i$ are very sensitive to $c_s$—particularly in the destabilized region of the flow, that is, $z/z_i \in (0.8, 0.95)$. Figure 10 illustrates that the disproportionate increase in the SGS heat fluxes in the destabilized zone reflects a disproportionate increase in $K_m$ (and hence $K_h$) with increasing $c_s$. Recall that $K_m \propto c_s^{4/3}$ is expected for flows in which the SGS buoyancy term is negligible and dis-

sipation is independent of $c_s$ (e.g., appendix B). Such scaling describes well the relationship between $K_m$ and $c_s$ in the bulk of the PBL but fails in the destabilized regions of the flow. Here increasingly peaked values of $K_m$ (with increasing $c_s$) result from increasingly negative values of the deformation Richardson number (e.g., Fig. 10b), that is increasingly important buoyancy terms in the SGS model. From the definition of $\mathrm{Ri}_D$ [in appendix B Eq. (B11)], we note that the peak in the magnitudes
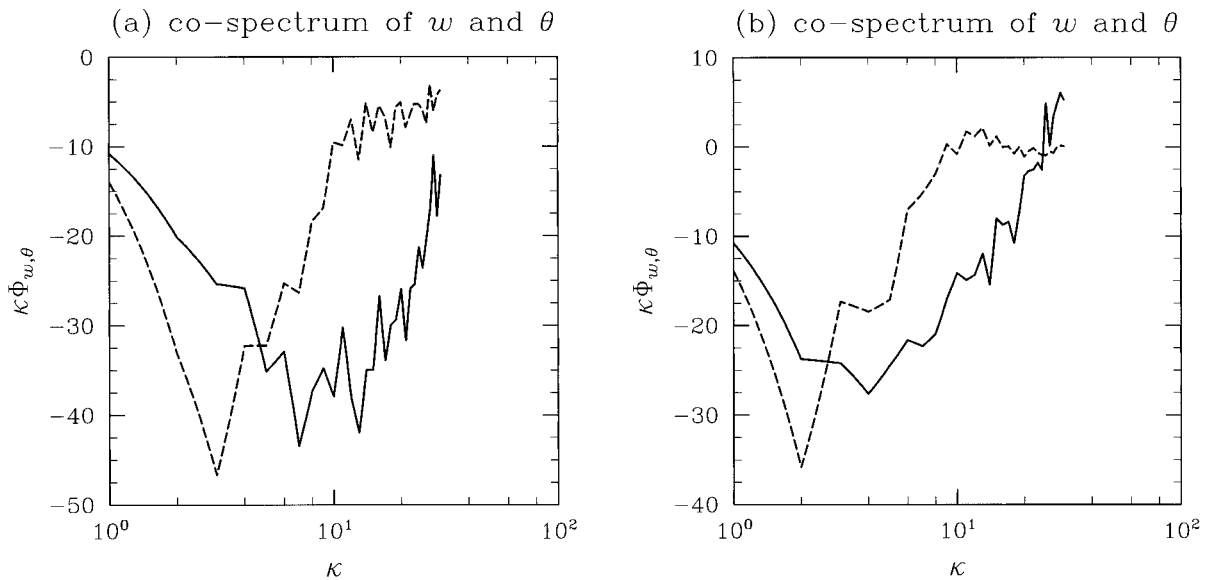


FIG. 9. Two-dimensional cospectra of $w$ and $\theta_*$, where $\theta_*$ is the value of $\theta$ interpolated, on the basis of our advection algorithms, to a $w$ point, and $\kappa = (\kappa_x^2 + \kappa_y^2)^{1/2}$. From SMK-S-064 class calculations. Solid line: $c_s = 0.15$; dashed line: $c_s = 0.35$. Cospectra at (a) height where minimum buoyancy flux locates, and (b) 10 m (2 levels) below this point.
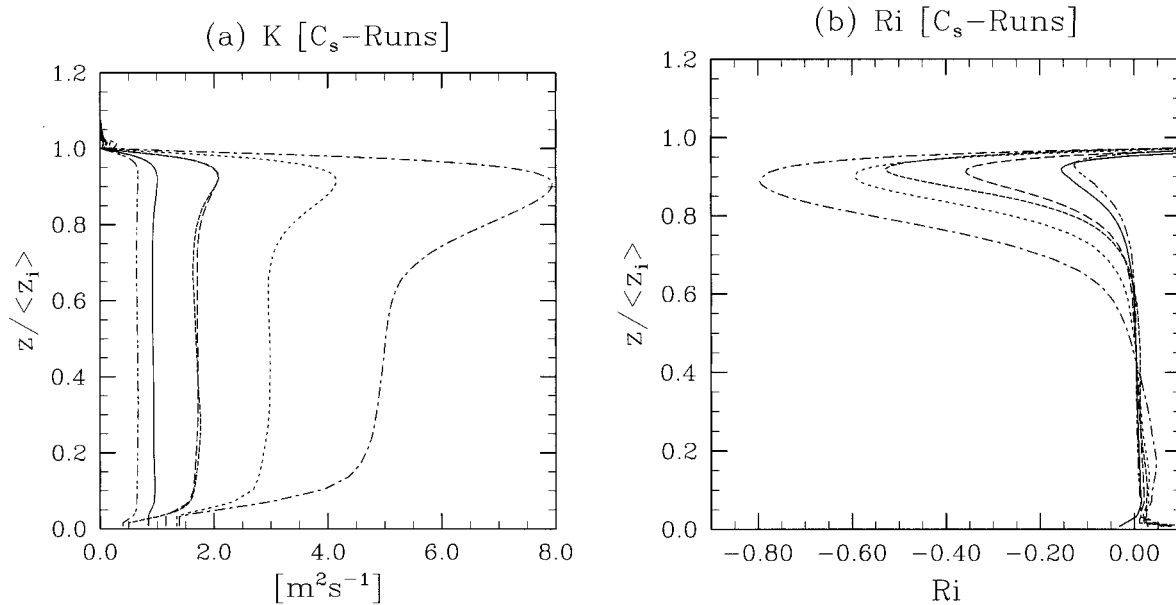
## (a) K [$C_s$–Runs]

## (b) Ri [$C_s$–Runs]

FIG. 10. Sensitivity of (a) $K_m$ and (b) $Ri_D$ to changes in $c_s$ for a suite of SMK-S-064 class calculations. Lines as in Fig. 7. Included for reference are results from some SMK-S-128 class simulations with $c_s = 0.23$ (dash–dot–dot), $c_s = 0.46$ (fine dots).

of $Ri_D$ and $K_m$ indicates $c_s$ more effectively damps the deformation (or shear production), thereby allowing SGS buoyancy production to play a larger role in the SGS–TKE budget. In retrospect this might have been anticipated; while the equilibrium value of $N^2$ largely reflects a balance between the resolved scales and the forcing, and is less affected by changes to $c_s$, the grid-scale deformation is determined by a balance between the large-scales and the dissipation, and is under more direct control by the SGS model.
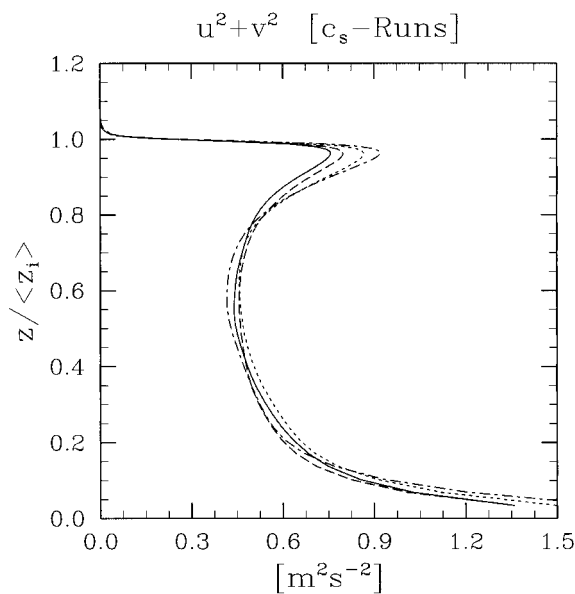
## $u^2 + v^2$ [$c_s$–Runs]

FIG. 11. Resolved variances in horizontal winds. Lines as in Fig. 7.

### 3) ON VELOCITY MOMENTS

The effect of $c_s$ on our calculations is not limited to thermodynamic fluxes and entrainment rates. For instance, Fig. 11 shows that increasing $c_s$ tends to produce a more pronounced upper PBL peak in the resolved variance of the horizontal velocity. Because the SGS energy is more-or-less constant this sensitivity projects onto the total variances as well. Although not shown, a further sensitivity to $c_s$ is evident in the structure of the vertical velocity skewness near the inversion. Increasing $c_s$ tends to result in a less pronounced maxima, similar to what is evident in Fig. 6b.

### b. The stability prefactor

The stability prefactor in the Smagorinsky model can be modified by either changing the value of $Ri_c$ or by altering the functional form of the term multiplying $(c_s\lambda)^2 S$ in Eq. (4). In our tests we consider both a modest change to the functional form of the prefactor, as well as the effects of changing $Ri_c$. In the latter (which we discuss first), we consider separate suites of experiments in which $Ri_c$ is alternately modified in the stable and destabilized regions of the flow, as this helps us better delineate the role of $Ri_c$.

By reducing $Ri_c$, for $Ri_D < 0$, we can artificially increase the eddy viscosity in the destabilized part of the flow, and thus selectively increase the amount of the forcing (or buoyancy flux) that is carried by the SGS model. Changes in $Ri_c$ sufficient to yield a twofold increase in the maximum value of the SGS heat flux have no noticeable effect on either the distribution of the vertical velocity at the inversion or on the resolved en-
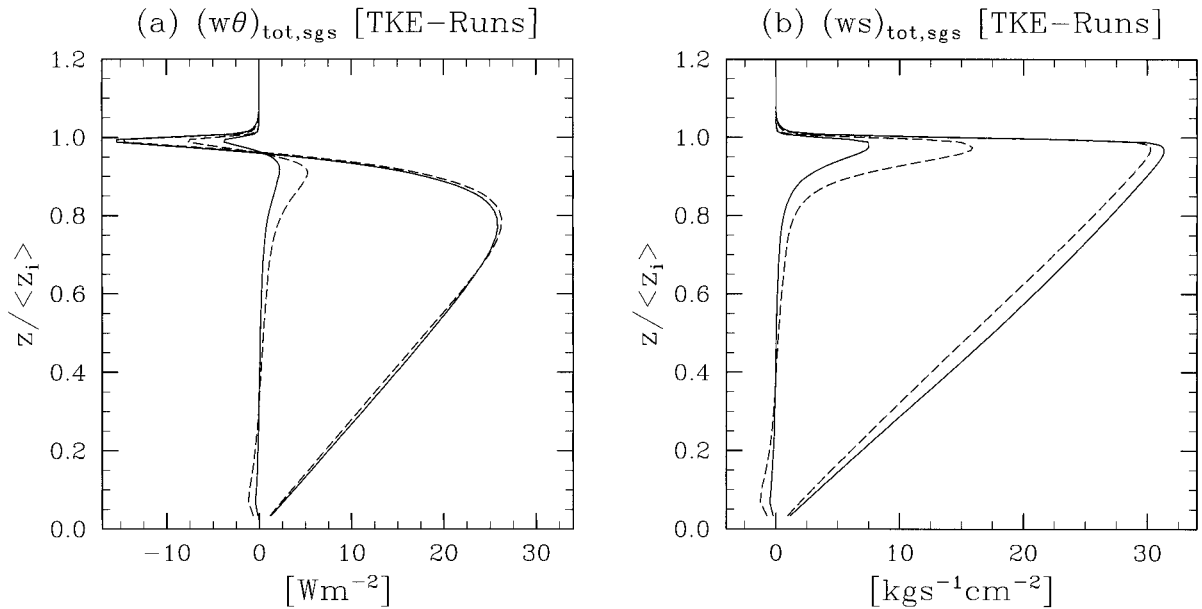
FIG. 12. Heat and smoke fluxes for SMK-T class calculations with $c_m = 0.1$ (solid) and $c_m = 0.25$ (dashed).

trainment. This indicates, somewhat surprisingly, that there is not a strong relationship between the amount of the buoyancy flux available for driving resolved-scale motions and the value of the resolved entrainment heat flux.

Changes to $\mathrm{Ri}_c$, for $\mathrm{Ri}_D > 0$, also have a minor influence on the overall flow, with most of the effect being limited to the actual value of the SGS heat flux at $z_i$. Experiments with $\mathrm{Ri}_c \in (\frac{1}{3}, \frac{1}{6}, \frac{1}{12})$ result in SGS heat fluxes of $(-2.0, -0.5, 0.0)$ W m$^{-2}$, respectively, with no discernible influence on the resolved heat flux. Because the SGS flux constitutes such a small fraction of the total flux at $z_i$, this change has little effect on the flow as a whole. Furthermore, unlike the effect of $c_s$ on entrainment, the $\mathrm{Ri}_c$ (for $\mathrm{Ri}_D > 0$) effect saturates if $\mathrm{Ri}_c$ becomes sufficiently small. The fact that these two effects (i.e., the $\mathrm{Ri}_c$ and $c_s$ effects) are independent are further supported by tests that show that the $c_s$ sensitivity is maintained even for a SGS model with $\mathrm{Ri}_c = 0$.

Mason (1989) has used the argument that the mixing length-scale should be reduced in stabilized portions of the flow to justify modifications to the form of the Smagorinsky model. In appendix B [i.e., Eq. (B14)] we show how a length-scale correction that accounts for possible stability effects results in a modified SGS model that approaches its cutoff Richardson number more rapidly. Using the Smagorinsky model cast in this form reduces the SGS contribution to the entrainment heat flux. Further tests designed to mimic the approach of the UKMO group were performed, in these tests instead of using Eq. (B14), we simply squared the stability term in Eq. (B13); that is, we write $K_m \propto (1 - \mathrm{Ri}_D/\mathrm{Ri}_c)$.[2] Such a change had an even less discernible effect on our solutions.

## 5. The Deardorff model

In attempting to see if the above delineated sensitivities are evident in calculations based on different algorithms (SGS and otherwise), we repeated the standard smoke cloud integration using the NCAR code. Because, in computing SGS fluxes, this code solves, following Deardorff (1980), an equation for $e$ (the SGS TKE) it is not possible to simply change $c_s$. Instead we change the value of $c_m$, which relates the eddy viscosity to a length scale and $\sqrt{e}$. In the local equilibrium limit $c_s \propto c_m^{3/4}$ (e.g., appendix B). SMK-T class integrations with the NCAR LES show little (if any) sensitivity of entrainment rates and thermodynamic fluxes to changes in $c_m$. In this respect the NCAR calculations behaved similarly to those by the WVU group Lewellen and Lewellen (1998).

To better understand what is causing the lack of sensitivity in LES with the NCAR code, we introduced a prognostic $e$ model into the CSU code. For the SGS length scale $\lambda$ both codes use $\lambda = (3/2)(\Delta x \Delta y \Delta z)^{1/3}$. In the CSU code $\Delta z$ varies with height, but for the purpose of the length scale computation it is held fixed at 7.4 m. Results from this calculation with the CSU model are shown in Fig. 12. The prognostic $e$ model effectively eliminates the sensitivity of entrainment to changes in the eddy viscosity.

Further calculations with the CSU code indicated that the basic sensitivity of the resolved-scale entrainment fluxes is preserved in calculations with the $e$ model, but what differs is the ability of the SGS fluxes to compensate. This is clearly evident in Fig. 12, where in the entrainment zone SGS heat fluxes contribute more substantially to the total entrainment flux, and are more

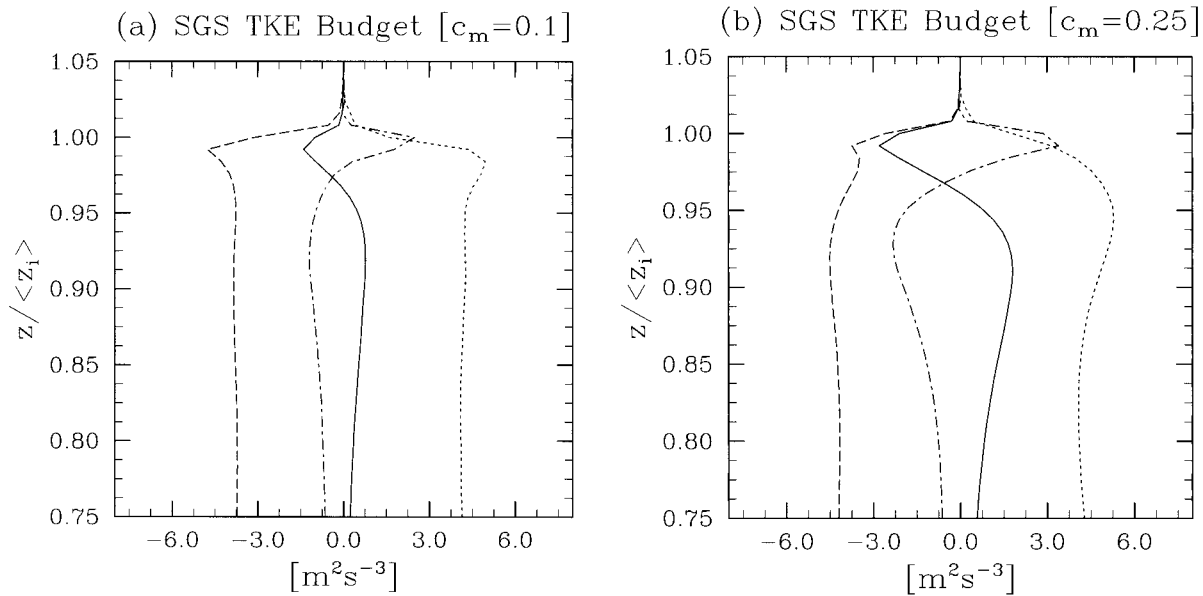## (a) SGS TKE Budget [$c_m$=0.1]



## (b) SGS TKE Budget [$c_m$=0.25]

Fig. 13. Budgets of SGS TKE from some SMK-T class simulations. Buoyancy production (solid line), shear production (dotted line), dissipation (dashed line), other terms (i.e., advective plus diffusive transport and storage terms) (dash–dot). Here $c_m = 0.1$, (upper panel), and $c_m = 0.25$ (lower panel).

sensitive than corresponding Smagorinsky model calculations to changes in the SGS model—although in the destabilized region around $0.9z_i$ the SGS fluxes are less sensitive to changes in the SGS model. The difference between the calculations mainly reflects, as it must, the nonlocal, nonequilibrium terms in the $e$ equation (i.e., the advective transport, the diffusive transport terms that model the third moments, and the storage term). As illustrated by the dash–dot lines in Fig. 13, the net contribution from these terms (which are neglected in the Smagorinsky model), are leading order in the entrainment zone and explain the increased value, and compensating sensitivity, of the SGS component of the entrainment heat flux (indicated by solid lines), as well as the reduction (relative to corresponding calculations with the Smagorinsky model) of the SGS heat flux around $0.9z_i$.

We conducted further simulations, in which we artificially modified the prognostic equation for $e$ so as to isolate and understand the effect of the three individual processes neglected in the Smagorinsky model. We found that each of the three terms were independently capable of providing the aforementioned compensating effect; although only the advective transport terms did so robustly. The ability of either diffusion-like terms (i.e., the modeled third moment terms in the prognostic equation for $e$) or nonequilibrium terms to effectively (and increasingly) transport $e$ into the inversion layer with increasing $c_m$ depended upon details of the numerical algorithm.

The effectiveness of the diffusive transport of $e$ depends on how $K_e$, the eddy diffusivity of $e$ is calculated. In both the NCAR and the CSU model $e$ is assumed,

following Mason (1989), to locate at layer interfaces (i.e., on $w$ points on the Arakawa C-grid template). Because $K_e$ is a function of $e$, diffusion calculations require averaging values of $K_e$ from layer interfaces to layer centers (i.e., from $w$ points to $\theta$ points). If this averaging is done arithmetically, that is, we solve for $K_e$ at level $k + \frac{1}{2}$ according to $2K_e^{k+1/2} = K_e^{k+1} + K_e^k$, the diffusive transport is effective (in the above described sense), but when the averaging is done geometrically, that is, $2/K_e^{k+1/2} = 1/K_e^{k+1} + 1/K_e^k$, as suggested for instance by Patankar (1980), the diffusive transport is ineffective. This sensitivity to averaging ultimately reflects the unsatisfactory resolution of cloud-top processes.

For the case of the nonequilibrium terms, we found that their effectiveness in the CSU model was evident only if the flow was horizontally dealiased using an upper one-thirds wave cutoff filter, as is routinely done in the NCAR model. The justification for doing so is that the small scales are well known to be contaminated by both aliasing and finite-difference errors. Recent attempts at quantifying these errors suggest that the energy in the error power spectrum may considerably exceed the energy in the SGS power spectrum at small scales (Ghosal 1996). Introducing a spectral cutoff filter into the CSU code results in a 50% reduction in $\overline{w'w'}$ at the inversion (reflecting the divergent nature of the $w$ spectra near and at the inversion),[6] it also significantly

---

[6] For archival purposes we also note here two further effects of spectral filtering: (i) the maximum of the horizontal variances below $z_i$ are reduced; (ii) the subgrid entrainment heat flux minimum tends to become more peaked in the inversion, as a result just below $z_i$
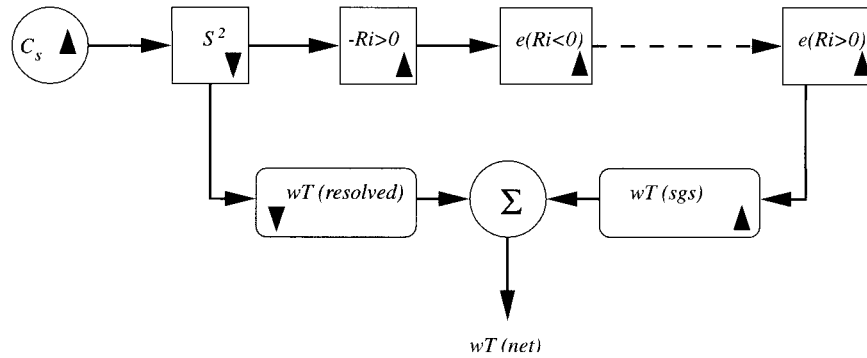
FIG. 14. A schematic relationship between $c_s$ (or any parameter setting an effective filter scale), resolved entrainment and SGS entrainment in SGS–TKE-based SGS models. The tendency of a field to increase or decrease with a change in $c_s$ is indicated by the direction of the triangles in the box, as well as the shading of the boxes.

lessens (by about a factor of 3, when using the prognostic $e$ code without transport or modeled third-order terms) the sensitivity of entrainment to changes in $c_m$. That is, when the spectral cutoff filter is used, the magnitude of SGS fluxes increase to compensate for reductions in resolved entrainment fluxes with increasing values of $c_m$, thus leading to a more robust solution.

## 6. Discussion

First let us emphasize that the sensitivities that we report here are, for the most part, modest. Moreover in a broad sequence of subsequent calculations such sensitivities were found to be weakened in lower $Ri_B$ flows (we did experiments with $\Delta\Theta = 4$ K and 2 K), when the forcing of the turbulence is moved to the surface as in the clear convective PBL, or if higher-order (but oscillatory) advection schemes are used to transport scalars. Nonetheless, our results are important because they demonstrate that the ability of the smoke cloud calculation to show convergence as a function of $c_s$, [or if we accept the arguments of Mason and Brown (1999), which our calculations largely corroborate, as a function of grid-spacing] depends to a great extent on the behavior of the SGS model.

In Fig. 14 we attempt to synthesize our findings schematically. Here we show that increasing $c_s$ tends to damp small-scale motions (as represented in the diagram by the magnitude of the deformation). This damping has two further consequences: (i) as the inversion region becomes less energetic (e.g., $\overline{w'w'}$ near $z_i$ is reduced, cf. Fig. 8a) resolved entrainment fluxes are reduced; and (ii) the magnitude of $Ri_D$ (where recall that $Ri_D \propto S^{-2}$) in the destabilized region of the flow is increased (cf. Fig. 10) resulting in greater production of $e$, as, for instance, evidenced by larger values of $K_m$ evident (cf.

Fig. 10) in the vicinity of $0.9z_i$. The dashed line in Fig. 14 is meant to indicate that this increased energy in the $Ri_D < 0$ part of the flow may, or may not (depending upon the assumptions in the SGS model), be available to other parts of the flow. When there is an integrating mechanism in the equation for $e$, that is, a mechanism for values of $e$ to influence their neighbors in space and time, then it may be possible for increased values of $e$ in the $Ri_D < 0$ parts of the flow to lead to larger value of $e$ in the $Ri_D > 0$ parts of the flow. In this case the SGS model may act, as we find to be the case of the Deardorff model, in a manner that compensates for resolved-scale sensitivities. This type of compensation would seem to be particularly favorable in flows like the smoke cloud, where very stable and slightly destabilized parts of the flow are in close proximity.

In section 4 we suggested, that physically, radiatively driven layers such as the smoke cloud may behave more rigidly than other flows. Our reasoning was that if something acted to change the entrainment rate the resolved energetics would change in a compensating manner, that is, less entrainment implies more TKE production, which then leads to more entrainment. Given this view we see that the feedback process is partially truncated by the Smagorinsky model; because enhanced production of $e$ just below the inversion cannot affect directly the budget of $e$ in the inversion, the production of more $e$ need not generate more SGS entrainment. Including advective or diffusive transport, or time-rate-of-change terms in the $e$ model extends, in a sense, this rigidity to the SGS model, thereby leading to apparently more robust solutions. Although we must be cautious here, physicality and robustness are different concepts, and one needs not imply the other. In the end, our inability to do extensive convergence tests makes it difficult to say what the correct answer is. At best we can say that our results explain contradictory sensitivities to horizontal resolution as reported by several groups, and warrant some degree of open-mindedness when evaluating the ability of LES to properly represent entrainment

resolved and subgrid fluxes are of opposite sign, an effect in better accord with the resolved cospectra just below $z_i$ (cf. Fig. 9b).

scalings in large $Ri_B$ flows. Two points we discuss further below.

### a. Entrainment rate sensitivities and previously published work

Recall that the LBL–UW group (Stevens and Bretherton 1999) report on calculations that exhibit a sensitivity to the horizontal resolution, but the calculations by the WVU group (Lewellen and Lewellen 1998) are remarkably insensitive to horizontal resolution. The fact that the WVU group used a prognostic $e$ model while the LBL–UW group used a Smagorinsky model is consistent with our results.[7] Our results are also consistent with the extensive number of sensitivity studies done by the WVU group. For example, the lack of sensitivity of the WVU calculations to the SGS model reflects the fact that despite the number of tests conducted, the only one that led to a significant sensitivity was the one that truncated the compensating mechanism we hypothesize to be present in their model, that is, those tests they call low Reynolds number tests, which are performed by setting the eddy diffusivity and viscosity to constant values (D. Lewellen 1998, personal communication). Last, our results are also consistent with the unpublished results of the UKMO group, who find a sensitivity to horizontal resolution in their model (they have conducted unprecedented, and unpublished simulations with 5-m uniform grid spacing), that is based on the Smagorinsky closure.

Sensitivities to the eddy viscosity and vertical resolution may also explain the differences among the high vertical resolution calculations discussed in the original smoke cloud intercomparison study. That the UKMO code has the smallest entrainment (Bretherton et al. 1999, their Fig. 10) is consistent with results presented at the Smoke Cloud Workshop, which indicated that the UKMO simulations were characterized by a much larger mean eddy viscosity just below the inversion. Although we have not focused on the effect of different representations of resolved modes (i.e., different advection schemes) this could in all likelihood also have some bearing on the differences among models—particularly in so far as the advection schemes preferentially damp or amplify small scales in the momentum budget.

Because our results also indicate that differently configured LES codes are able to support different entrainment rates, it should not be surprising that entrainment heat flux ratios (upon which the process partitioning model of entrainment rests) differ among models—even

---

[7] Calculations that use no SGS model (or for which the SGS model is not relied upon to provide the dissipation), but rely on limiters in the advection algorithms to dissipate energy and bound the flow should (because of their inherently local nature), according to our arguments, behave more like calculations based on the Smagorinsky model.

if they are robust for individual models. Consider our results with the Smagorinsky model: depending on the effective viscosity near the inversion, one can arrive at different values of the ratio of the entrainment heat flux to the extrapolated heat flux (i.e., $a/b$ in the terminology of Fig. 1). A larger mean eddy viscosity tends to favor smaller ratios, as we find that $a/b$ varies from 0.42 to 0.25 as $c_s$ is increased from 0.15 to 0.53. These differences are on the order of the differences discussed in the introduction.

### b. Can we rule out the importance of small scales?

With regard to our second statement (regarding open-mindedness), recall that most LESs share a highly parametric representation of the SGS heat flux whose fidelity is largely untested. The second-order equation for the SGS heat flux in a Boussinesq fluid is as follows:

$$\frac{\partial}{\partial t}(\overline{u'_i \theta'}) = -\frac{\partial}{\partial x_k}(\overline{u_k}\,\overline{u'_i \theta'}) - \overline{u'_k \theta'}\frac{\partial \overline{u_i}}{\partial x_k} + \delta_{i3}\frac{g}{\theta_0}\overline{\theta'^2}$$
$$- \frac{\partial}{\partial x_k}\left(\overline{u'_i u'_k \theta'} + \frac{\delta_{ik}}{\rho_0}\overline{p'\theta'}\right) - \epsilon_\theta,$$
$$-\overline{u'_i u'_k}\frac{\partial \overline{\theta}}{\partial x_k} + \frac{1}{\rho_0}\overline{p'\frac{\partial \theta'}{\partial x_i}}, \quad (6)$$

where $\epsilon_\theta$ represents the effect of molecular processes. With few exceptions LES models used to study PBL turbulence assume that the dominant balance is between the last two terms on the rhs of (6) and that all other terms are negligible. Furthermore, because the pressure scrambling term (the last term on the rhs) must be parameterized, it is assumed that it functionally attempts to return the flow to isotropy and hence is proportional to the SGS heat flux. This assumption results in a simple, downgradient model for the SGS heat flux; that is,

$$\overline{u'_i \theta'} \propto \frac{1}{\rho_0}\overline{p'\frac{\partial \theta'}{\partial x_i}} = \overline{u'_i u'_k}\frac{\partial \overline{\theta}}{\partial x_k}, \quad (7)$$

which in the end helps produce equilibrium limits for the models with cutoff values of $Ri_D$. Seemingly innocuous and physically justifiable changes to the SGS model, such as arguing that the variance production term is important, and including a simple model of it, can lead to the elimination of this cutoff Richardson number behavior, with dramatic implications for the overall behavior of the simulation in the entrainment zone (Sommeria 1976).

Although the model of the heat flux described above may be justified (or perhaps does not matter) within a well-developed inertial range, its validity is open to question within a poorly represented entrainment zone—particularly when the entrainment zone is characterized by large gradients and variances in the buoyancy variable as well as diabatic processes [not included in Eq. (6)].
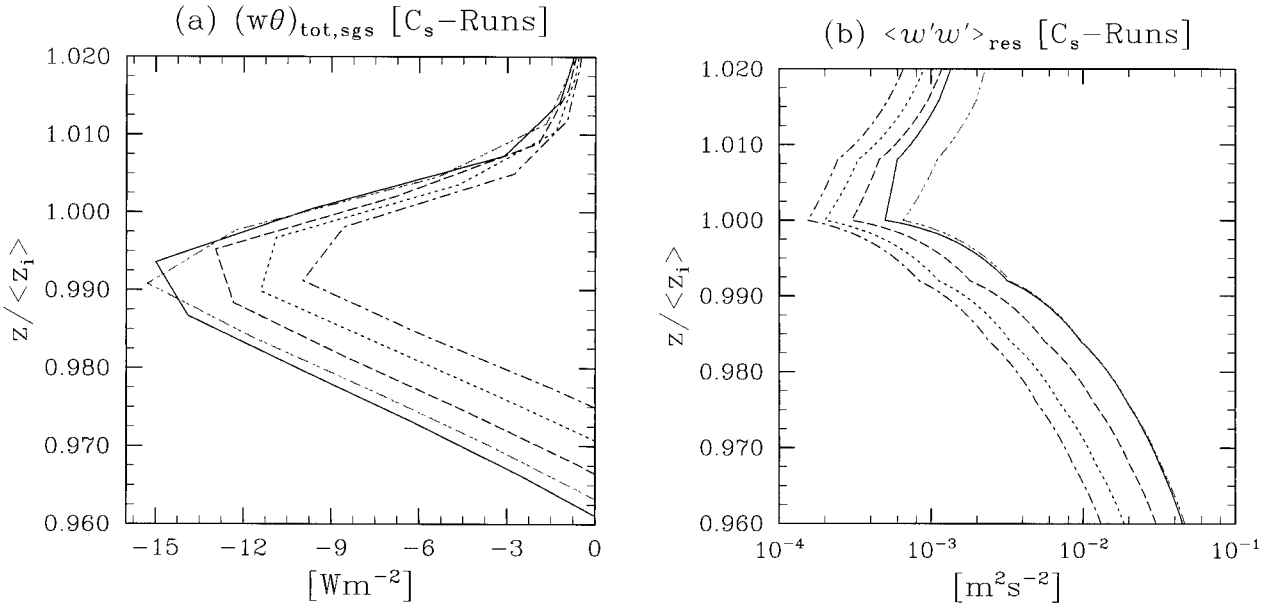
FIG. 15. (a) Entrainment heat fluxes and (b) vertical velocity variances from SMK-S-064 class simulations with $c_s = 0.15$ (solid), 0.23 (dashed), 0.35 (dotted), 0.53 (dash–dot), and an SMK-S-128 class simulation with $c_s = 0.23$.

Another reason for open-mindedness is that our flow analysis fails to reveal clearly identifiable structures, or processes, associated with entrainment. This may well be a failure of our analysis, but there are a number of indications that the sharp gradients, and the poor resolution of interfacial processes, affects the solutions one gets. Moreover, given our finding that the sensitivity, or the tendency toward convergence of a calculation, depends on the assumptions made in the SGS model, it seems fair to speculate that robust balances in various models might in the end be artifacts of the model numerics, peculiarities in the flow configuration, and SGS model assumptions.

Yet a further reason for open-mindedness is that it remains unclear as to what component of the total entrainment heat flux is truly resolved. As discussed in section 2c, flow analysis does not support the conclusion (based on a partitioning of the flux between the SGS and resolved component) that most of the entrainment heat flux is resolved. Indeed, *we cannot even rule out* the possibility that numerical diffusion plays a leading role in determining the amount of resolved entrainment.

For the sake of argument, consider a first-order upwind advection scheme (which makes up the diffusive limit for most monotone methods). A Taylor series expansion of such a scheme indicates that the leading-order truncation errors take a diffusive form, with diffusivity

$$K_{upwind} = \frac{w\Delta z}{2} \qquad (8)$$

and associated diffusive flux

$$\overline{w\theta}_{upwind} \approx -K_{upwind}\frac{\partial\theta}{\partial z}. \qquad (9)$$

In Fig. 15, we plot the value of the vertical velocity variance $\sigma_w^2(z_i)$ and the entrainment heat flux at the inversion from a number of different simulations. This figure illustrates that $\sigma_w^2(z_i)$ is correlated with the entrainment heat flux. Taking $\sigma_w(z_i)$ to be a characteristic velocity of inversion undulations, and assuming that the stratification in this region is between 0.5 and 1 K m$^{-1}$ across the 5-m vertical grid (e.g., Fig. 8), yields

$$-15 < \overline{w\theta}_{upwind} < -4 \text{ W m}^{-2}. \qquad (10)$$

This rough attempt to bound the diffusive component of the resolved flux suggests that it is of the same order as the total resolved flux. While it might be an extreme assumption to expect our scheme to behave like an upwind scheme at the inversion all of the time, undulation velocities at the interface could conceivably exceed our estimates. In light of this analysis, and the results presented at the end of section 4a(1), we find it difficult to rule out the possibility that purely numerical effects account for a significant component of the resolved entrainment heat flux.

In the end, our results further argue for the need to test the entrainment relationships derived from LES. These tests should include much higher resolution simulations, a specially designed field campaign, and continually refined laboratory measurements.

## 7. Summary

Our major findings are twofold:

• Increased values of the eddy viscosity result in smaller

values of the resolved entrainment heat flux, which, depending on the behavior of the SGS model, may or may not result in changes to the net entrainment rate.

- Because the reduction of the resolved entrainment through enhanced eddy viscosities in the upper part of the PBL tends to be associated with greater production of SGS TKE ($e$), models that allow for the $e$ at a point in space and time to be influenced by values of the $e$ at neighboring points (e.g., Deardorff's SGS model and most variants) are better able to compensate for the sensitivities of the resolved-scale entrainment heat fluxes.

In addition we try to show how, for modest changes in the horizontal mesh, the SGS viscosity in the entrainment zone acts as a proxy for horizontal resolution. Our results suggest that the horizontal sensitivity reported in simulations by the LBL–UW group but absent in the calculations by the WVU group reflect different assumptions used in their SGS models. Consequently, in flows such as the smoke cloud (where commonly used resolutions poorly resolve processes in the entrainment zone) the robustness, or lack thereof, of previously reported results may have less to do with physical processes, and more to do with uncertain assumptions made in the numerical, and SGS models.

If the sensitivities we report here end up representing the degree of our uncertainty in representing entrainment in LES, then we are in good shape. Given the limitations in our understanding of a variety of other processes, an uncertainty in parameterized entrainment rates of less than 50% is certainly tolerable. However, given the uniformity of approach in most LES models, our inability to rule out numerical diffusion as contributing significantly to the resolved entrainment, and the lack of a good theory for the behavior of small-scale turbulence in the stratified entrainment zone, only time, and further work, will tell if the sensitivities discussed here are accurate measures of our current uncertainty.

## APPENDIX A

### Description of the CSU Model and its Algorithms

The solver used was developed out of the architectural framework of the mesoscale model developed at Colorado State University (Pielke et al. 1992). It uses finite differences to approximate the following system of equations in a Cartesian coordinate system, that is, $x_i = (x, y, z)$:

$$\frac{\partial u_i}{\partial t} = -\frac{1}{\rho_0}\frac{\partial(\rho_0 u_j u_i)}{\partial x_j} - c_p \theta_0 \frac{\partial \phi}{\partial x_i} + g(\theta^* - \overline{\theta^*})\delta_{i3}$$
$$+ \frac{1}{\rho_0}\frac{\partial}{\partial x_j}\left[\rho_0 K_m \left(\frac{\partial u_i}{\partial x_j} + \frac{\partial u_j}{\partial x_i}\right)\right] \tag{A1}$$

$$\frac{\partial \theta^*}{\partial t} = -\frac{1}{\rho_0}\frac{\partial(\rho_0 u_j \theta^*)}{\partial x_j} - \frac{1}{c_p \rho_0}\frac{\partial F_r}{\partial x_3}$$
$$+ \frac{1}{\rho_0}\frac{\partial}{\partial x_j}\left[\rho_0 K_h\left(\frac{\partial \theta^*}{\partial x_j}\right)\right] \tag{A2}$$

$$\frac{\partial s}{\partial t} = -\frac{1}{\rho_0}\frac{\partial(\rho_0 u_j s)}{\partial x_j} + \frac{1}{\rho_0}\frac{\partial}{\partial x_j}\left[\rho_0 K_h\left(\frac{\partial s}{\partial x_j}\right)\right], \tag{A3}$$

where $s(x_i, t)$ is the concentration of an optically thick tracer that we refer to as "smoke," $\theta^*(x_i, t) = \theta(x_i, t) - \theta_0$ is the thermodynamic variable (here potential temperature), $u_i(x_i, t)$ is the vector velocity ($u$, $v$, $w$), $\phi(x, y, z, t)$ is the pressure variable, $\rho_0(z)$ is the basic-state density, $\theta_0$ is a fixed basic-state potential temperature, $c_p = 1004$ J K$^{-1}$ is the isobaric specific heat of dry air, and $g = 9.8$ m s$^{-2}$ is the gravitational acceleration. In the diffusive-like terms on the rhs of each equation $K_m$ and $K_h$ may be thought of as a flow-dependent eddy viscosity, diffusivity, respectively. The dependent variables of the system, that is, ($u_i$, $\theta^*$, $s$) are all assumed to be suitably smooth so that they contain no information on scales smaller than the discretization.

In the anelastic system, continuity requires that

$$\frac{\partial(\rho_0 u_j)}{\partial x_j} = 0. \tag{A4}$$

This constraint along with the condition that $w = 0$ on the upper and lower boundaries allows us to uniquely determine $\phi$ as a function of other variables. Hence we see that we have a fully coupled system of equations as the forcing

$$F_r(s, z) = F_0 \exp\left(-\kappa \int_z^\infty \rho_0 s \, dz\right) \tag{A5}$$

is a function of height and the integrated smoke concentration. For the smoke cloud the cloud-top gradient

in $F_r$ drives the flow, which allows us to specify a zero flux (i.e., free slip for momentum) surface boundary for all variables.

The equations are solved using finite differences. The momentum equations are marched forward by a leapfrog scheme with an Asselin filter while scalar terms are integrated using a forward-in-time method. Advection terms in the momentum equation are solved using fourth-order centered differences except in regions of grid stretching where second-order centered differences are used. In the scalar equations, advection terms are calculated in one of two ways. One method uses the fourth-order generalization of the Lax–Wendroff differences (Tremback et al. 1987), the other method interpolates between the fourth-order fluxes and a first-order scheme in order to ensure monotonicity in the solution (Zalesak 1979). The former scheme is variance friendly, the latter is variance diminishing. Pressure is solved in Fourier space in the horizontal and by inverting a tridiagonal system in the vertical. We periodically check to ensure that the solver satisfies the continuity equation to machine accuracy throughout the course of a simulation. The equations are solved on a staggered (Arakawa C) grid, which is compressed and or stretched in the vertical. Integrations with a fine vertical mesh throughout were compared to integrations with a compressed mesh near the top of the PBL and a stretched mesh above the PBL. Sensitivities to the moderate stretching ratios (1.1) used were looked for, but not found. The eddy diffusivity is calculated following the procedure outlined by Mason (1989), similarly, to avoid vertical averaging of SGS viscosities and diffusivities, the SGS TKE is collocated with $w$ on the staggered mesh. Boundary conditions are periodic in $x$ and $y$. Boundary conditions at the top of the domain are constant gradient for scalar variables and free slip for momentum.

## APPENDIX B

### SGS Models

#### a. Prognostic SGS–TKE models

The starting point for most SGS models used in LES of the PBL is the equation for the unresolved turbulent kinetic energy, $e = \frac{1}{2}\overline{u_i'u_i'}$,

$$\frac{\partial e}{\partial t} = -\frac{1}{\rho_0}\frac{\partial(\rho_0\overline{u}_j e)}{\partial x_j} - \frac{\partial(\rho_0\overline{u_i'e} + \overline{u_i'p'})}{\partial x_i} - \overline{u_i'u_j'}\frac{\partial\overline{u}_i}{\partial x_j}$$
$$+ \frac{g}{\theta_0}\overline{w'\theta'} - \epsilon, \qquad (B1)$$

here written under the anelastic approximation with $\rho_0(z)$ being the basic-state density and $\epsilon$ representing dissipation. Only the advective transport term (the first term on the rhs) is explicitly represented, all other terms must be modeled. Typically stresses and strains are assumed to align,

$$\overline{u_i'u_j'} = -K_m D_{ij}, \quad \text{where } D_{ij} = \frac{\partial\overline{u}_i}{\partial x_j} + \frac{\partial\overline{u}_j}{\partial x_i}, \quad \text{and}$$

$$K_m = c_m l e^{1/2}. \qquad (B2)$$

Scalar fluxes are assumed to be downgradient, for instance, the heat flux is given by

$$\overline{u_i\theta} = -K_h\frac{\partial\overline{\theta}}{\partial x_i}, \quad \text{with } K_h = c_h l e^{1/2}, \qquad (B3)$$

while the third-moment terms are modeled diffusively,

$$\frac{\partial(\rho_0\overline{u_i'e} + \overline{u_i'p'})}{\partial x_i} = -2K_m\frac{\partial e}{\partial x_i}. \qquad (B4)$$

Last, the dissipation is assumed proportional to the three-halves power of the energy,

$$\epsilon = c_\epsilon e^{3/2}/l. \qquad (B5)$$

The above models for the SGS energy equation yields a closed set of equations given values for $c_\epsilon$, $c_m$, $c_h$, and a length scale $l$. The length scale is often related to a generalized measure of the grid spacing, which we denote by $\lambda$, and/or the local stability.

In the absence of stability corrections (i.e., in the homogeneous isotropic limit)

$$c_\epsilon = \pi\left(\frac{2}{3\alpha}\right)^{3/2}, \qquad c_m = \frac{1}{\pi}\left(\frac{2}{3\alpha}\right)^{3/2},$$

$$c_h = \frac{4}{3\gamma}\frac{1}{\pi}\left(\frac{2}{3\alpha}\right)^{1/2} \qquad (B6)$$

can be derived for steady-state solutions to the SGS–TKE equation with a minimal number of other assumptions (Lilly 1967; Moeng and Wyngaard 1989; Schmidt and Schumann 1989; Schumann 1991). In Eq. (B6), $\alpha$ and $\gamma$ are the coefficients in the spectra of the energy variance and temperature variance, respectively. Choosing $\alpha = 1.6$, and $\gamma = 1.34$ (Schumann 1991) yields $(c_\epsilon, c_m, c_h) = (0.845, 0.0856, 0.204)$.

In the presence of stability, $l$ is limited,

$$l = \min(l_s, \lambda), \quad \text{where } l_s = c_l\left(\frac{e^{1/2}}{N}\right), \quad \text{and}$$

$$N^2 = \frac{g}{\theta_0}\frac{\partial\overline{\theta}}{\partial z}. \qquad (B7)$$

By assuming isotropy and equating $l_s$ with the distance a parcel of velocity $w' = \sqrt{(2/3)e}$ would travel in an environment with stability $N^2$, we can derive $c_l = \sqrt{2/3} = 0.82$. In addition $c_h$ and $c_\epsilon$ are often given a stability dependence,

$$c_\epsilon = c_{\epsilon 1} + c_{\epsilon 2}\left(\frac{l}{\lambda}\right), \qquad c_h = c_{h1} + c_{h2}\left(\frac{l}{\lambda}\right). \qquad (B8)$$

If we require that for $l = \lambda$ (the neutral limit) $c_h$ and $c_\epsilon$ regain their values in neutrally stratified flows only

two new constants are introduced. These are fixed by assuming that in the very stable limit, $c_h = c_m$, and that the local equilibrium model has a Richardson number cutoff of $Ri_c = 0.23$. The first condition implies that $c_{h1} = c_m$, the second implies that

$$c_{\epsilon 1} = c_m c_l^2 (Ri_c^{-1} - 1). \tag{B9}$$

These stability corrections are necessary when using the prognostic SGS–TKE model. In the absence of such corrections entrainment rates and SGS fluxes are dramatically altered. This differs from some previous studies (e.g., Schumann 1991) and what we found using the Smagorinsky model (cf. section 5b). These issues have been investigated further and are discussed in more detail by Stevens et al. (1999).

In presenting the above closure assumptions we have not endeavored to defend their veracity. Indeed it has long been known that fundamental aspects of these equations are fallacious (e.g., Clark et al. 1979). But in many respects, the fallacy of some assumptions does not appear to have a dramatic effect on the fidelity of many aspects of the flow (Schmidt and Schumann 1989; Mason 1989; Nieuwstadt et al. 1991). Thus we are less interested in whether the SGS model is correct, and more interested in whether it is incorrect in a way that matters.

### b. Equilibrium models

By neglecting transport and time-rate-of-change terms in Eq. (B1) one assumes that dissipation is locally balanced by conversion of mean flow energy into SGS TKE. In this limit Eq. (B1) takes the form:

$$c_m l e^{1/2} S^2 - c_h l e^{1/2} N^2 = c_\epsilon \frac{e^{3/2}}{l}, \quad \text{where}$$

$$S^2 = \frac{\partial \overline{u}_i}{\partial x_j} D_{ij}. \tag{B10}$$

In the absence of stability corrections (i.e., $l$ constant), Eq. (B10) can be solved for $e$,

$$e = \frac{S^2}{\pi^2} \left[ 1 - \frac{c_h}{c_m} Ri_D \right], \quad \text{where } Ri_D = \frac{N^2}{S^2}, \quad \text{and}$$

$$Pr = \frac{c_m}{c_h}. \tag{B11}$$

Here we have used the fact that $c_m/c_\epsilon = \pi^{-2}$. Also note that the turbulent Prandtl number behaves like a Richardson number cutoff as energies must be positive definite. In the case when the length scale is corrected for stability effects as reviewed above, the equilibrium solution becomes

$$e = \frac{c_m c_l}{c_{\epsilon 2} + c_{h2} c_l^2} \left( \frac{\lambda^2 S^4}{N^2} \right)^2 \left[ 1 - \frac{c_m c_l^2 + c_{\epsilon 1}}{c_m c_l^2} Ri_D \right]^2. \tag{B12}$$

In the case where $l = \lambda$, Eq. (B11) and the definition of $K_m$ imply that

$$K_m = (C_s \lambda)^2 S \sqrt{1 - \frac{Ri_D}{Pr}}, \tag{B13}$$

where $C_s = (c_m^3/c_\epsilon)^{1/4}$ is the Smagorinsky constant. Equation (B13) is just the traditional Smagorinsky model. It is used often as the closure model for our calculations. In the well-mixed (i.e., $N^2 \to 0$ limit) constant dissipation limit we note that (B10) implies that for $K_m$ defined according to (B13), and for a fixed length scale $l$, $S \propto C_s^{-2/3}$ or equivalently $K_m \propto C_s^{4/3}$.

In the case of stability corrections, where $l = l_s$ the eddy viscosity can be written in the form

$$K_m = \frac{(c_m c_l)^3 \lambda^2}{(c_{\epsilon 2} + c_{h2} c_l^2)^2} \left( \frac{S}{Ri_D^{3/2}} \right) \left[ 1 - \frac{c_m c_l^2 + c_{\epsilon 1}}{c_m c_l^2} Ri_D \right]^2. \tag{B14}$$

This model, in that it approaches the $Ri_D$ cutoff as $(1 - Ri_D/Ri_c)^2$, is similar to the model proposed by Mason (1989) although it differs through the introduction of a $Ri_D^{-3/2}$ term, different values of constants, and by the fact that it is introduced only when $l_s < \lambda$, whereas Mason introduces his stability corrected form for $N^2 > 0$.

### APPENDIX C

### Spurious Radiative–Dynamical Interactions

We consider an idealized situation in which an interface capping a turbulent underlying smoke fluid moves steadily through our vertical domain. We suppose that the entrainment process is layerwise and diffusive, that is it is characterized by a successive replacement of the lowest layer of smokefree, warmer, "free tropospheric" fluid by smoke-full, cooler, turbulent boundary layer fluid. We further suppose that the rate of growth of the smoke layer ($w_e = dz_i/dt$) is, in the absence of other affects, set externally, perhaps by the large-scale energetics of the underlying fluid, as for instance is advocated by Lewellen and Lewellen (1998). As shown from our flow snapshot in Fig. 2 and by the PDF of maximum temperature gradients in Fig. 8b, even for $\Delta x = 25$ m and $\Delta z = 5$ m, the interface is to a first approximation confined to one or two grid levels. This view of the interface is corroborated by the snapshots of a similar flow at higher resolution (e.g., Stevens and Bretherton 1999), the almost stepwise growth of the height of the minimum buoyancy flux (e.g., Fig. 4 in Lock and MacVean 1998), as well as results from the original smoke cloud intercomparison (Bretherton et al. 1999). Simulations performed with coarser vertical or horizontal resolution, are presumably even better characterized by this model.

From this discrete perspective, entrainment corresponds to a progressive change in the state of the grid cell, or the layer of grid cells, of vertical extent $\Delta z$ located directly above $z_i$. Denoting this state by the couplet $\{\theta, s\}$, symbolizing potential temperature and smoke mixing ratio, respectively, entrainment takes the grid cells in question from an initial state $\{\theta^+, s^+\}$,

corresponding to the quiescent upper fluid, to a final state, $\{\theta^-, s^-\}$, corresponding to the properties of the turbulent lower fluid. That is, if the lower fluid were to expand steadily through the grid in a time interval $\Delta t$ where

$$\Delta t \equiv \frac{\Delta z}{w_e}, \tag{C1}$$

the temperature and the smoke mixing ratio of the grid cell in question would change with time according to

$$\frac{d}{dt}\{\theta, s\} = -\frac{1}{\Delta t}\{\Delta\Theta, \Delta S\}, \quad \text{for } 0 \le t \le \Delta t, \tag{C2}$$

where

$$\Delta\Theta \equiv \theta^+ - \theta^- \quad \text{and} \quad \Delta S \equiv s^+ - s^-, \tag{C3}$$

and throughout we neglect effects associated with small vertical gradients in density and the time rate of change of the state of the lower fluid. Equation (C2) follows from the fact that at any time $t \in [0, \Delta t]$ the grid cell in question should be seen as being composed of a fraction $t/\Delta t$ of lower fluid and a fraction $1 - t/\Delta t$ of upper fluid.

Because the discretized version of the radiative equation (A5) does not account for the position of an interface within a grid cell, it cannot partition the radiative cooling between clear and cloudy elements *within* a grid cell. Thus, in partially cloudy grid cells, clear and cloudy parts of the grid cell are cooled indiscriminantly. Furthermore, when the air in a cloud-top/inversion-base grid cell is composed of both PBL air and above inversion air, its mean temperature will generally be warmer than the underlying PBL air, and thus it will be stably stratified. If the location of the cloud top could be (or were) tracked within a grid cell, the grid cell could be split into a clear and cloudy part reflective of the respective states of the overlying and underlying layers. The cooling would then be initially focused in the cloudy portion, but because the cloudy part of the grid cell will not in general be thermally separated from the lower part of the PBL, any cooling that occurs within it would be distributed by turbulence throughout the PBL as a whole. Thus, the temperature of the cloudy portion would remain at $\theta^-$ and the temperature of the clear portion would remain equal to $\theta^+$, and consistent with our neglect of changes with time in the state of the PBL as a whole (i.e., by assuming that the PBL is sufficiently deep such that $|d\theta^-/dt| \ll |d\theta/dt|$) the average radiative cooling in the layer would be negligible. Consequently we see that by failing to account for the position of the cloud-top interface within a grid cell the cooling is focused in the entrainment layer, instead of being dispersed through the PBL. That is, instead of the change of state of those grid cells being "entrained" being governed by (C2), it instead is described by

$$\frac{d\theta}{dt} = \frac{-\Delta\Theta}{\Delta t} - \frac{1}{c_p\rho_0\Delta z}[F_0 - F_0\exp(-\rho_0\kappa s\Delta z)] \tag{C4}$$

$$\frac{ds}{dt} = \frac{-\Delta S}{\Delta t}, \tag{C5}$$

where the largely spurious radiative cooling effect is now present. Equations (C4) and (C5) provide a basis for asking how does the time, $t_*$, it takes $\theta(t)$ to go from $\theta^+$ to $\theta^-$ compare to the time (i.e., $\Delta t$) it would take in the absence of spurious cooling in the radiatively ambiguous layer? Or equivalently, how does the ratio $R \equiv t_*/\Delta t$ depend upon the parameters of the problem (i.e., $w_e$, $F_0$, $\kappa$, $\Delta z$)?

Given the simple manner in which we constructed the problem, the solution is straightforward. Integrating the equation for $s$ leads to

$$s(t) = s^+ - \Delta S\left(\frac{t}{\Delta t}\right), \tag{C6}$$

which when substituted into (C4), recalling that $s^+ = 0$ and $\Delta S = -1$, yields

$$\frac{d\theta}{dt} = \frac{-\Delta\Theta}{\Delta t} - \frac{1}{c_p\rho_0\Delta z}\left[F_0 - F_0\exp\left(-\rho_0\kappa\Delta z\frac{t}{\Delta t}\right)\right], \tag{C7}$$

which can be readily integrated. The analysis below becomes simpler if we here consider approximate solutions obtained by linearizing the exponential term before integrating (a good approximation in the limit of small $\kappa s\Delta z$, which in our case is always smaller than 0.1 and 0.25 for $\Delta z = 5$ and 25 m, respectively) so that

$$\theta(t) - \theta^+ \approx -\frac{\Delta\Theta}{\Delta t}t - \frac{\kappa F_0}{2\Delta t c_p}t^2. \tag{C8}$$

Recalling our definition of $t_*$ to be that time such that $\theta(t_*) = \theta^-$ yields

$$\Delta\Theta = \frac{t_*}{\Delta t}\Delta\Theta + \frac{\kappa F_0\Delta t}{2c_p}\left(\frac{t_*}{\Delta t}\right)^2. \tag{C9}$$

Equation (C9) demonstrates how the cooling is due to two terms, the entrainment term, which is the first term on the rhs, and the radiative term. The coefficient in the radiative term always enhances the cooling, and depends explicitly on the grid spacing (recall that $\Delta t \equiv \Delta z/w_e$). If the radiative forcing were dependent only on the average concentration of the smoke, this grid spacing dependence would vanish, but because the spurious cooling depends on the smoke path, larger grid cells will cool more through this effect than will composites of smaller grid cells. Physically this follows because the fraction of the cooling, which on average is focused in the inversion layer, depends on the thickness of the layer, and in the absence of a well-resolved interface (i.e., an interface whose undulations are much larger than the grid spacing) this is defined to be $\Delta z$. While on the one hand this is a nice feature, because it allows the effect

to vanish as $\Delta z \to 0$, it also introduces an explicit resolution sensitivity into the entrainment rate.

This explicit sensitivity is best illustrated by solving (C9) for $R = t_*/\Delta t$:

$$R(\Delta z; \xi) = -\frac{\xi}{\Delta z} + \sqrt{\frac{\xi}{\Delta z}\left(\frac{\xi}{\Delta z} + 2\right)}, \quad \text{where}$$

$$\xi = -\frac{c_p w_e \Delta\Theta}{\kappa F_0}, \tag{C10}$$

where in the definition of $\xi$ we have used (C1), that is, $\Delta t \equiv \Delta z/w_e$. In the special case that $\xi/\Delta z \to \infty$, corresponding to the situation of either fine vertical resolution, relatively rapid entrainment or negligible radiative effects (i.e., $\kappa$ or $F_0 \to 0$), $R \to 1$, as one would expect. For the case of $\xi/\Delta z \to 0$ corresponding to the limit of coarse vertical resolution, rapid entrainment, or relatively strong radiative effects, $R \to 0$, which implies that all of the entrainment is spuriously driven by radiation.

More typical situations live between these two limits. For instance, in the case studied in this paper $\kappa = 0.02$ m$^2$ kg$^{-1}$, $\Delta\Theta \approx 4$ K (as taken from the mode of the distribution in Fig. 8b with $\Delta z = 5$ m), $F_0/c_p \approx 0.06$ K kg m$^{-2}$ s$^{-1}$, and $w_e \approx 0.0025$ m s$^{-1}$ (e.g., corresponding to experiment 304.2 in Table 2) yields $\xi = 8.33$. From (C10) it follows that $R(25) \approx 0.54$ and $R(5) \approx 0.81$, thus implying an increase in entrainment rate between a $\Delta z = 5$ m calculation and a $\Delta z = 25$ m calculation of 45%. Entrainment rate ratios between the 5- and 25-m calculations by the UKMO, WVU, and ARAP models [i.e., $R(25)/R(5) - 1$] are 46% as reported by Bretherton et al. (1999).[8] The extent of agreement is probably fortuitous; there is a certain amount of arbitrariness in specifying $\Delta\Theta$, for instance, choosing $\Delta\Theta = 7$ K leads to a somewhat smaller prediction of $R(25)/R(5) - 1 = 33\%$. Moreover our use of a linearized exponential function for the radiative flux is actually an upper bound on the effect. Because our model indicates that setting a threshold on the minimum smoke path necessary for radiation to become active can effectively eliminate the cooling in the radiatively ambiguous layer, it provides an explanation for the reduced sensitivity to vertical resolution in calculations that set a critical smoke path threshold of about $s \approx 0.5\Delta z$ before radiative fluxes become active.[9] This effect is not explained by competing ideas (e.g., Stevens and Bretherton 1999;

Bretherton et al. 1999). Overall the degree of explanatory power of the model, and its physical and quantitative basis lead us to believe that it is the most plausible explanation for the sensitivity of smoke cloud simulations to vertical resolution.

The simple model here has been developed for mostly heuristic purposes. It can obviously be extended by considering analogous models for simulations of water clouds (for which case the total-water mixing ratio must exceed the saturation threshold before liquid water is produced and the layer becomes radiatively active), or by considering its effect given more realistic models of $w_e$, or by considering similar effects associated with other processes (e.g., subsidence, C. S. Bretherton and H. Grenier 1998, personal communication; Lenderink et al. 1999). A further interesting extension follows by supposing that the buoyancy flux scales with a radiatively based bulk Richardson number (e.g., Lock and MacVean 1999)

$$w_e \approx A\frac{F_0}{c_p\Delta\Theta}\rho_0, \tag{C11}$$

with $A$ a constant of proportionality, in which case, $\xi \approx A/(\kappa\rho_0)$, which says that the above-mentioned spurious effect scales with the ratio of the optical depth of the absorbing medium to the grid spacing.

Last, we emphasize that while the purely spurious effect discussed here may make entrainment rates artificially sensitive to vertical resolution in poorly resolved smoke cloud simulations, this should not be confused with in some senses a similar (albeit physical) effect associated with radiative cooling in the time-mean interfacial layer of finite thickness evident, for instance, in simulations with well-resolved cloud-top undulations (Moeng et al. 1999).

---

[8] We picked these calculations because they were the only ones that used a 5-m vertical grid in their high vertical resolution calculations. The CSU and NCAR high-resolution simulations were performed with $\Delta z = 12.5$ m.

[9] These calculations were first presented by Hans Cuijpers, and subsequently reproduced by us. Hans Cuijpers deserves credit for originally proposing what essentially amounts to this explanation. Peter Duynkerke is thanked for his tireless (and in the end contagious) advocacy of essentially these ideas.

REFERENCES

Bretherton, C. S., and Coauthors, 1999: An intercomparison of radiatively driven entrainment and turbulence in a smoke cloud, as simulated by different numerical models. *Quart. J. Roy. Meteor. Soc.,* **125,** 391–423.

Clark, R. A., J. H. Ferziger, and W. C. Reynolds, 1979: Evaluation of subgrid-scale models using an accurately simulated turbulent flow. *J. Fluid Mech.,* **91,** 1–16.

Deardorff, J. W., 1980: Stratocumulus-capped mixed layers derived from a three-dimensional model. *Bound.-Layer Meteor.,* **18,** 495–527.

——, G. E. Willis, and B. H. Stockton, 1980: Laboratory studies of the entrainment zone of a convectively mixed layer. *J. Fluid Mech.,* **100,** 41–64.

Ghosal, S., 1996: An analysis of numerical errors in large-eddy simulations of turbulence. *J. Comput. Phys.,* **125,** 187–206.

Kraus, E. B., 1963: The diurnal precipitation change over the sea. *J. Atmos. Sci.,* **20,** 551–556.

Lenderink, G., M. C. vanZanten, and P. G. Duynkerke, 1999: Can an e–l turbulence closure simulate entrainment in convective boundary layers? *J. Atmos. Sci.,* **56,** 3331–3337.

Lewellen, D., and W. Lewellen, 1998: Large-eddy boundary layer entrainment. *J. Atmos. Sci.,* **55,** 2645–2665.

Lilly, D. K., 1967: The representation of small-scale turbulence in numerical simulation experiments. *IBM Scientific Computing*

*Symp. on Environmental Sciences,* Yorktown Heights, NY, IBM DP Division, 195–210.

——, 1968: Models of cloud topped mixed layers under a strong inversion. *Quart. J. Roy. Meteor. Soc.,* **94,** 292–309.

Lock, A. P., and M. K. MacVean, 1999: A parametrization of entrainment driven by surface heating and cloud-top cooling. *Quart. J. Roy. Meteor. Soc.,* **125,** 271–300.

Mason, P., 1989: Large eddy simulation of the convective atmospheric boundary layer. *J. Atmos. Sci.,* **46,** 1492–1516.

——, and A. R. Brown, 1999: On subgrid models and filter operations in large eddy simulations. *J. Atmos. Sci.,* **56,** 2101–2114.

Moeng, C.-H., 1984: A large-eddy simulation for the study of planetary boundary layer turbulence. *J. Atmos. Sci.,* **41,** 2052–2062.

——, and U. Schumann, 1991: Composite structure of plumes in stratus-topped boundary layers. *J. Atmos. Sci.,* **48,** 2280–2291.

——, P. P. Sullivan, and B. Stevens, 1999: Including radiative effects in an entrainment rate formula for buoyancy-driven PBLs. *J. Atmos. Sci.,* **56,** 1031–1049.

——, and J. C. Wyngaard, 1989: Spectral analysis of large-eddy simulations of the convective boundary layer. *J. Atmos. Sci.,* **45,** 3573–3587.

Nieuwstadt, F. T. M., P. J. Mason, C. H. Moeng, and U. Schumann, 1991: Large-eddy simulation of the convective boundary layer: A comparison of four computer codes. *Selected Papers From the 8th Symposium on Turbulent Shear Flows,* Springer-Verlag, 343–367.

Patankar, S. V., 1980: *Numerical Heat Transfer and Fluid Flow. Series in Computational Methods in Mechanics and Thermal Sciences.* McGraw Hill, 197 pp.

Pielke, R. A., and Coauthors, 1992: A comprehensive meteorological modeling system—RAMS. *Meteor. Atmos. Phys.,* **49,** 69–91.

Rouse, H., and J. Dodu, 1955: Turbulent diffusion across a density discontinuity. *Houille Blanche,* **10,** 522–532.

Sayler, B. J., and R. E. Breidenthal, 1998: Laboratory simulations of radiatively induced entrainment in stratiform clouds. *J. Geophys. Res.,* **103,** 8827–8837.

Schmidt, H., and U. Schumann, 1989: Coherent structure of the convective boundary layer derived from large-eddy simulations. *J. Fluid Mech.,* **200,** 511–562.

Schumann, U., 1991: Subgrid length-scales for large-eddy simulation of stratified turbulence. *Theoret. Comput. Fluid Dyn.,* **2,** 279–290.

Sommeria, G., 1976: Three-dimensional simulation of turbulent processes in an undisturbed trade wind boundary layer. *J. Atmos. Sci.,* **33,** 216–241.

Stevens, B., W. R. Cotton, G. Feingold, and C.-H. Moeng, 1998: Large-eddy simulations of strongly precipitating, shallow, stratocumulus-topped boundary layers. *J. Atmos. Sci.,* **55,** 3616–3638.

——, C.-H. Moeng, and P. P. Sullivan, 1999: Entrainment and subgrid lengthscales in large-eddy simulations of atmospheric boundary layer flows. *Developments in Geophysical Turbulence,* R. Kerr and Y. Kimura, Eds., Kluwer, in press.

Stevens, D., and C. S. Bretherton, 1999: Effects of resolution on the simulation of stratocumulus entrainment. *Quart. J. Roy. Meteor. Soc.,* **125,** 425–439.

Sullivan, P. P., J. C. McWilliams, and C.-H. Moeng, 1996: A grid nesting method for large-eddy simulation of planetary boundary-layer flows. *Bound.-Layer Meteor.,* **80,** 167–202.

——, C.-H. Moeng, B. Stevens, D. H. Lenschow, and S. D. Mayor, 1998: Entrainment and structure of the inversion layer in the convective planetary boundary layer. *J. Atmos. Sci.,* **55,** 3042–3064.

Tremback, C., J. Powell, W. R. Cotton, and R. A. Pielke, 1987: The forward-in-time upstream advection scheme: Extension to higher orders. *Mon. Wea. Rev.,* **115,** 3540–555.

Turner, J. S., 1986: Turbulent entrainment: The development of the entrainment assumption, and its application to geophysical flows. *J. Fluid Mech.,* **173,** 431–471.

vanZanten, M. C., P. G. Duynkerke, and J. W. M. Cuijpers, 1999: Entrainment parameterization in convective boundary layers derived from large eddy simulations. *J. Atmos. Sci.,* **56,** 813–828.

Zalesak, S. T., 1979: Fully multidimensional flux-corrected transport algorithms for fluids. *J. Comput. Phys.,* **31,** 335–362.